Slippage effect on the dispersion coefficient of a passive solute in a pulsatile electro-osmotic flow in a microcapillary

J. Muñoz,[1] J. Arcos,[1,*] O. Bautista,[1,†] and F. Méndez[2]
[1]*Instituto Politécnico Nacional, Avenida de las Granjas 682, Colonia Santa Catarina, Azcapotzalco, Ciudad de México 02250, Mexico*
[2]*Universidad Nacional Autónoma de México, Coyoacan, Ciudad de México 04510, Mexico*

(Received 14 September 2017; published 23 August 2018)

The hydrodynamic dispersion of a neutral solute released into a pulsatile electro-osmotic flow in a microcapillary that is affected by slippage at the wall (modeled by the Navier slip condition) is studied theoretically. The long-time Taylor dispersion is analytically derived using the homogenization method with multiple scales. The results indicate that the effective dispersion coefficient depends on a dimensionless slip length, an angular Reynolds number, the amplitude of the oscillatory component of the external electric field, and an electrokinetic parameter that relates the radius of the microcapillary with the Debye length. Our results suggest that in the presence of the Navier slip condition, the dispersivity is maximized by up to two orders of magnitude compared with that obtained through the classical no-slip condition.

DOI: 10.1103/PhysRevFluids.3.084503

I. INTRODUCTION

The mechanism for the dispersion of a passive solute cloud in a fluid flow through a tube is of great interest for predicting the rate of broadening of pollutants through a circular channel or the spread of soluble salts in the bloodstream. The latter was the motivation under which Taylor [1] provided us with the first description of this phenomenon as an enhanced diffusion process in the flow direction caused by the combined actions of axial convection and transversal diffusion across a tube. The term dispersion is intended to distinguish this process from a true molecular diffusion process [2] and it has a close relationship with the flow properties. The subsequent work conducted by Aris [3] using the method of moments generalized the dispersion study to any pressure-driven periodic flow pattern through a circular tube. Thus, the Aris-Taylor theory has become the cornerstone of many studies related to the transport, separation, and mixing of species with physiological, environmental, or chemical applications. Chatwin [4] analyzed how a passive contaminant disperses along the axis of a tube in which the flow is driven by a longitudinal pressure gradient varying harmonically with time. Watson [5] found that the resulting flux of the diffusing substance along a pipe depends on the cross section and can be analytically evaluated from any frequency of oscillation if the pipe is circular or if it is a two-dimensional channel. A few studies have focused on determining the dispersion coefficient of oscillatory flows in two- and three-dimensional rectangular channels. In this context, Lee *et al.* [6] observed that the presence of the channel wall in the third dimension gives rise to a dispersion coefficient that is approximately seven times higher than that of the two-dimensional flow. The presence of the sidewalls could significantly increase dispersion in oscillatory flows in two- and three-dimensional rectangular channels [7]. They concluded that the maximum

*jarcos@ipn.mx
†obautista@ipn.mx

increment in dispersion occurs at very low frequencies, at which the flow can be considered to be pseudounidirectional with a slowly changing velocity.

In recent years, the dispersion mechanism has found an important application in the mixing and separation of chemical species that govern the performance of labs on a chip (LOCs) [8–13]. In many cases, the design and construction of LOCs are based on electrokinetic phenomena, and LOCs have become a subject of considerable interest due to their potential to provide significant advantages in chemical analyses, medical diagnostics, and environmental monitoring compared to the conventional ways in which these fields have been addressed. For example, LOCs have the ability to handle low fluid volumes, lower manufacturing costs, and flexibility for automated operation. In this context, many works have been performed to demonstrate the importance of ac electro-osmosis as a valuable mechanism for manipulating microflows based on the interaction of the electric double layer (EDL) with an externally applied alternating electric field [14–17]. The resulting flow, which is known as an ac electro-osmotic flow [ac-driven electro-osmotic flow (EOF)], has important relevance for the mixing [18] and mass separation of species [19] due to the strong dependence among the oscillation frequency of the imposed electric field, the EDL thickness, the solute transport properties, and the resulting dispersion. Currently, the research work focused on the oscillatory EOF dispersion has considered not only the sole influence exerted by the alternating electric field but also the notable influence of physicochemical processes [20,21] and nonuniform potentials [22] at the walls of microconduits, thereby providing additional approaches to enhance or adjust the rate of spread of a solute.

The aforementioned investigations focusing on determining the effective dispersion coefficient caused by oscillatory EOFs assume the no-slip condition at the fluid-microchannel wall interface. Nevertheless, recent studies have considered the Navier slip boundary condition $\mathbf{u}_s = \lambda_N\{\bar{\bar{\gamma}} \cdot \mathbf{n} - [(\bar{\bar{\gamma}} \cdot \mathbf{n}) \cdot \mathbf{n}]\mathbf{n}\}$, where $\mathbf{u}_s$ is the fluid velocity at the wall, $\mathbf{u}$ is the velocity field, λ_N denotes the Navier slip length, $\mathbf{n}$ represents the unit vector normal to the microchannel surface pointing toward the fluid, and $\bar{\bar{\gamma}}$ is the rate of strain tensor, which is given by $\bar{\bar{\gamma}} = \nabla\mathbf{u} + (\nabla\mathbf{u})^T$. The Helmholtz-Smoluchowski velocity u^s_{HS} under the slippage condition is obtained as

$$u^s_{\mathrm{HS}} = -\frac{\epsilon\zeta E_0}{\mu}\left(1 + \frac{\lambda_N}{\lambda_D}\right), \tag{1}$$

where ϵ, ζ, E_0, μ, and λ_D are the permittivity of the electrolyte solution, the zeta potential at the surface of a microchannel, the external electric field, the dynamic viscosity, and the Debye length, defined as $\lambda_D = (\epsilon k_B T/2e^2 z^2 n_\infty)^{1/2}$, respectively. Here e, k_B, n_∞, and T are the electron charge, the Boltzmann constant, the ionic number concentration, and the absolute temperature, respectively. As shown in Eq. (1), by considering the slippage as the boundary condition, the mean velocity through the microchannel can be notably increased compared with the classical Helmholtz-Smoluchowski velocity according to the value of the ratio λ_N/λ_D. In this context, several studies have focused on the effect of slippage on the hydrodynamics of EOFs [23,24] and on determining the hydrodynamic effective dispersion coefficient in an EOF driven by a dc by including the slippage [11,25]. These studies are the only ones that have taken the effect of slippage on the dispersion in EOFs into account. Hydrodynamic slippage has been shown to be a topic of fundamental physical interest that has the potential to exert important repercussions in many areas of engineering and applied sciences where liquids interact with small-scale systems [26,27]. In the electrokinetic scenario, such repercussions have been reflected in significant changes in the EDL dynamics [28,29] and in a notable enhancement in the driven volumetric flow rates through a large slip-induced flow amplification [8,24,30,31].

In this paper, recognizing the inherent potential of pulsatile electro-osmotic flows (PEOFs) as an important means for electro-osmotic mass flow control or enhancement [15,22,32–34] and considering that the surface of microchannel walls can be hydrophobic, we determine the effective dispersion coefficient, also known as Taylor dispersion, in the long timescale of the process, i.e., when the transient stage has died out and the flow field corresponds to the periodic transient motion. Quantitative surprises emerge from this study, showing that the dispersion coefficient can be notably

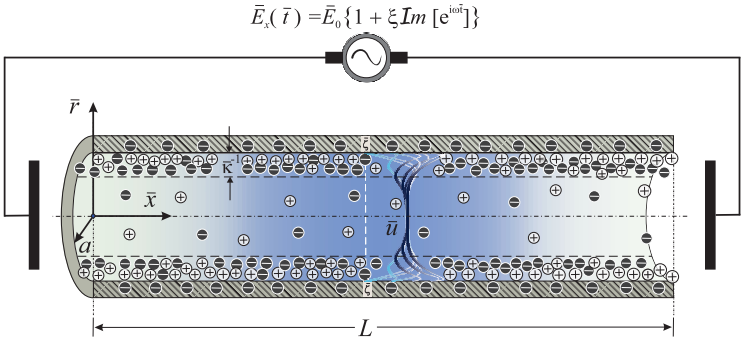

FIG. 1. Schematic diagram of the physical model under study.

increased due to a PEOF when slippage is considered. These effects should be taken into consideration when analyzing and designing microchannels. In this context, the present study aims to broaden the understanding of the influence and importance of the oscillatory EOFs and the Navier slip condition in terms of the mass transport phenomenon. To this end, this study analyzes the importance of the variations in the rate of change of a pulsatile body force over the rate of spread of a solute immersed in an EOF through a microcapillary with and without slippage at the wall. This study also evaluates the importance of the EDL thickness on the mass transport mechanism, showing that the PEOF with $\kappa \gg 1$ is a strong candidate to participate in the separation of chemical species, which is one of the major fluidic processes to be performed in lab-on-a-chip systems.

II. PROBLEM FORMULATION

A qualitative schematic of the physical model under study is presented in Fig. 1. The dispersion of an analyte band along a microcapillary, with slippage and a low surface potential ζ at its inner surface, caused by a PEOF is considered. The origin of the cylindrical coordinate system (x, r) is located at the left end and at the center of the microcapillary, as shown in the schematic. The radius of the microcapillary is denoted by a and its length is denoted by L. In this context, we define a parameter $\beta = a/L \ll 1$ that will be useful for our mathematical modeling. The fluid is a symmetric electrolyte solution z:z, where z is the valence of the electrolyte, and an EDL is formed on the inner surface of the microcapillary. The variable notation used throughout this paper is defined as follows: If a variable is decorated with an overbar (e.g., $\bar{\gamma}$), then it represents a physical quantity; otherwise, it is a dimensionless variable (e.g., γ). The PEOF is caused by applying a pulsating potential difference between the ends of the microcapillary, generating an external pulsating electric field; accordingly, an electric force on the ions of the electrolyte is generated. The external electric field is assumed to be of the form $\bar{E}_x(t) = \bar{E}_0\{1 + \xi\,\mathrm{Im}[e^{i\omega\bar{t}}]\}$, where $\bar{E}_0$ is the steady part of the electric field, $\xi\,\mathrm{Im}[e^{i\omega\bar{t}}]$ denotes the harmonically fluctuating part, ξ is a factor such that ξE_0 represents the amplitude of the oscillatory part of the electric field, and ω represents the angular frequency of the oscillation. Moreover, $\mathrm{Im}[F]$ represents the imaginary part of the complex quantity F and $i = \sqrt{-1}$. By considering a dimensionless time t, which is normalized using the inverse of the angular frequency $1/\omega$, as a characteristic time and $E_x(t) = \bar{E}_x(\bar{t})/\bar{E}_0$, the dimensionless form of the external electric field is given by

$$E_x(t) = \{1 + \xi\,\mathrm{Im}[e^{it}]\}. \tag{2}$$

The PEOF is assumed to be unidirectional and fully developed, characterized for a velocity distribution $\bar{u}(\bar{r}, \bar{t})$, and affected by slippage at the inner surface of the microcapillary. This type of PEOF was previously analyzed by Rojas *et al.* [32], who derived the dimensionless velocity

distribution

$$u(r,t) = u_s(r) + \mathrm{Im}[u_\omega(r)e^{it}], \tag{3}$$

where the dimensionless velocity is $u(r,t) = \bar{u}_x(\bar{r},\bar{t})/u_{\mathrm{HS}}$ and the Helmholtz-Smoluchowski velocity is defined as $u_{\mathrm{HS}} = -\epsilon\zeta E_0/\mu$ [35]. Here ϵ and μ are the dielectric permittivity and the dynamic viscosity of the electrolyte solution, respectively. In addition, $u_s(r)$ and $u_\omega(r)$ are the steady and oscillatory components of the dimensionless velocity profile, respectively, defined as

$$u_s(r) = 1 - \frac{I_0(\kappa r)}{I_0(\kappa)} + \kappa\delta\frac{I_1(\kappa)}{I_0(\kappa)}, \tag{4}$$

with

$$u_\omega(r) = \left\{\frac{\xi\kappa^2(\kappa^2 + iR_\omega)}{\left(\kappa^4 + R_\omega^2\right)I_0(\kappa)}\left[\frac{[I_0(\kappa) + \delta\kappa I_1(\kappa)]I_0(\sqrt{iR_\omega}r)}{I_0(\sqrt{iR_\omega}) + \delta\sqrt{iR_\omega}I_1(\sqrt{iR_\omega})} - I_0(\kappa r)\right]\right\}. \tag{5}$$

In the above expressions for the velocity field, I_0 and I_1 are the zeroth- and first-order modified Bessel functions of the first kind [36]. Note that κ is an electrokinetic parameter that is inversely proportional to the Debye length $\lambda_D = \kappa^{-1}$ and its dimensionless form is given by $\kappa = \bar{\kappa}a$. Here e, k_B, n_∞, and T are the electron charge, the Boltzmann constant, the ionic number concentration, and the absolute temperature, respectively. In addition, $R_\omega = \omega a^2/\nu$ is the angular Reynolds number [37], where ν is the kinematic viscosity of the fluid. Further, δ is the ratio between the Navier length λ_N and the microchannel radius, i.e., $\delta = \lambda_N/a$ and $r = \bar{r}/a$.

We consider that the fluid is moving with a velocity profile given by Eq. (3), and at instant $\bar{t} = 0$ (a condition not shown in Fig. 1), a pulse of a neutral solute is injected across the microcapillary. At sufficiently large times, i.e., $\bar{t} \gg O(a^2/D)$ (where D represents the molecular diffusivity of the solute in the electrolyte solution), this pulse has spread along the microcapillary axis through a process that enhances its effective diffusion in the direction of the flow known as Aris-Taylor dispersion, which exists because of the velocity shear across the microcapillary. Our objective is to analyze this long-scale behavior and derive an analytical expression for the dispersion coefficient that will allow us to understand how the hydrodynamic slippage, the angular frequency of the oscillatory part of the electric field together with its amplitude, and the EDL thickness affect the effective dispersion coefficient.

We consider the convection-diffusion equation that governs the behavior of a solute in an isotropic medium, which is given by

$$\frac{\partial\bar{C}}{\partial\bar{t}} + \frac{\partial(\bar{u}\bar{C})}{\partial\bar{x}} = D\left[\frac{\partial^2\bar{C}}{\partial\bar{x}^2} + \frac{1}{\bar{r}}\frac{\partial}{\partial\bar{r}}\left(\bar{r}\frac{\partial\bar{C}}{\partial\bar{r}}\right)\right], \tag{6}$$

with boundary conditions given by

$$\frac{\partial\bar{C}}{\partial r} = 0 \quad \text{at } r = 0, a. \tag{7}$$

Here $\bar{C}$ is the concentration (mass of species per bulk volume) of the diffusing substance. To obtain the dispersion coefficient, it is necessary consider that the species transport described by Eq. (6) occurs at different timescales and that the solute does not axially spread as fast as it would radially spread at the microcapillary; hence, we are in the presence of a multiple-scale phenomenon. To derive the effective dispersion coefficient for a PEOF in the periodic stage with slippage at the wall of the microcapillary, we use the homogenization method [38–40], which has been widely applied to analyze the dispersion phenomenon of passive solutes in pressure-driven flows.

Homogenization method

For convenience, we present the homogenization method to derive an expression that allows us to evaluate the dispersion coefficient, which will be obtained from the convection-diffusion equation (6),

also known as dispersivity, denoted by $\mathcal{D}$. For the analysis, we focus on the transport at a scale L that is considerably greater than the radius of the microcapillary a, i.e., we assume that the microcapillary radius is very small such that the transversal diffusion is completed within an oscillation period, i.e., $2\pi/\omega \sim a^2/D \sim O(1)$.

Under the above assumptions, the dimensionless form of Eq. (6) takes the form

$$\frac{\partial C}{\partial t} + \beta\,\mathrm{Pe}u(r,t)\frac{\partial C}{\partial x} = \beta^2\frac{\partial^2 C}{\partial x^2} + \frac{1}{r}\frac{\partial}{\partial r}\left(r\frac{\partial C}{\partial r}\right), \quad 0 < r < 1, \tag{8}$$

where $u(r,t)$ is the dimensionless velocity profile of a PEOF with slippage at the inner surface of the microcapillary wall and is given by Eq. (3). The dimensionless concentration distribution is $C = \bar{C}/C_R$, where C_R is a reference concentration. In addition, $x = \bar{x}/L$, $t = \bar{t}D/a^2$, and $\mathrm{Pe} = u_{\mathrm{HS}}a/D$ is the Péclet number, which is assumed to be of $O(1)$. In this context, we have considered some typical values of the physical parameters used in EOFs for estimating the dimensionless parameters involved in this study as follows: $\lambda_D \sim 10^{-9}$ m, $E_0 \sim 10^3\,\mathrm{V\,m^{-1}}$, $L \sim 10^{-2}$ m, $a \sim 10^{-6}$ m, $D \sim 10^{-9}\,\mathrm{m^2\,s^{-1}}$, $\lambda_N \sim 10^{-6}$ m, $\zeta \sim 10^{-2}$ m, and $u_{\mathrm{HS}} < 2 \times 10^{-3}\,\mathrm{m\,s^{-1}}$.

In the present problem, there are three timescales: a^2/D for the transversal diffusion, L/u_{HS} for the convection along L, and L^2/D for the diffusion along L for the convection-diffusion equation. Therefore, by introducing the three time coordinates

$$t_0 = t, \quad t_1 = \beta t, \quad t_2 = \beta^2 t \tag{9}$$

and proposing the perturbation series for the dimensionless concentration

$$C = C_0 + \beta C_1 + \beta^2 C_2 + \cdots \tag{10}$$

into Eq. (8) and after collecting terms of like powers in β, the following set of equations is obtained.

(i) The $O(\beta^0)$ problem. At this order, the governing equation is given by

$$\frac{1}{r}\frac{\partial}{\partial r}\left(r\frac{\partial C_0}{\partial r}\right) = 0, \tag{11}$$

subject to the boundary conditions

$$\frac{\partial C_0}{\partial r} = 0 \quad \text{at } r = 0, 1. \tag{12}$$

Here we have neglected the shortest time dependence for C_0 because we focus on the long behavior after the periodicity is completed. Accordingly, C_0 does not depend on r and it is of the form

$$C_0 = C_0(x, t_1, t_2). \tag{13}$$

(ii) The $O(\beta)$ problem. The dimensionless convection-diffusion equation for C_1 is governed by the problem

$$\frac{\partial C_1}{\partial t_0} + \frac{\partial C_0}{\partial t_1} + \mathrm{Pe}\{u_s + \mathrm{Im}[u_\omega e^{it_0}]\}\frac{\partial C_0}{\partial x} = \frac{1}{r}\frac{\partial}{\partial r}\left(r\frac{\partial C_1}{\partial r}\right), \tag{14}$$

with the boundary conditions

$$\frac{\partial C_1}{\partial r} = 0 \quad \text{at } r = 0, 1. \tag{15}$$

(iii) The $O(\beta^2)$ problem. At this order, C_2 is governed by

$$\frac{\partial C_2}{\partial t_0} + \frac{\partial C_1}{\partial t_1} + \frac{\partial C_0}{\partial t_2} + \mathrm{Pe}\{u_s + \mathrm{Im}[u_\omega e^{it_0}]\}\frac{\partial C_1}{\partial x} = \frac{\partial^2 C_0}{\partial x^2} + \frac{1}{r}\frac{\partial}{\partial r}\left(r\frac{\partial C_2}{\partial r}\right), \tag{16}$$

with the boundary conditions

$$\frac{\partial C_2}{\partial r} = 0, \quad r = 0{,}1. \tag{17}$$

Considering that our interest is after the transients have died out, i.e., the periodic response, the time average during one period of oscillation of any function f is defined as $\hat{f} = \frac{1}{2\pi}\int_0^{2\pi} f\, dt_0$. Therefore, time averaging Eqs. (14) and (15) yields

$$\frac{\partial C_0}{\partial t_1} + \mathrm{Pe} u_s \frac{\partial C_0}{\partial x} = \frac{1}{r}\frac{\partial}{\partial r}\left(r\frac{\partial \hat{C}_1}{\partial r}\right), \tag{18}$$

with the boundary conditions

$$\frac{\partial \hat{C}_1}{\partial r} = 0 \quad \text{at } r = 0, 1. \tag{19}$$

In this way, an inhomogeneous and steady boundary-value problem for $\hat{C}_1$ is obtained. The development of Eq. (18) continues. By defining the area average of a dimensionless quantity f as $\langle f \rangle = 2\int_0^1 r\, f\, dr$, the cross-sectional average of Eq. (18) is given by

$$\frac{\partial C_0}{\partial t_1} + \mathrm{Pe}\langle u_s \rangle \frac{\partial C_0}{\partial x} = 0. \tag{20}$$

According to the homogenization method, Eq. (20) represents a solvability condition for the inhomogeneous boundary-value problem for $\hat{C}_1$ given by Eq. (18). Subsequently, we subtract Eq. (20) from Eq. (14), thereby obtaining

$$\frac{\partial C_1}{\partial t_0} + \mathrm{Pe}\{\tilde{u}_s + \mathrm{Im}[u_\omega e^{it_0}]\}\frac{\partial C_0}{\partial x} = \frac{1}{r}\frac{\partial}{\partial r}\left(r\frac{\partial C_1}{\partial r}\right), \tag{21}$$

where $\tilde{u}_s = \bar{\tilde{u}}_s / u_{\mathrm{HS}}$ represents the deviation of the dimensionless velocity from its corresponding mean velocity, i.e., $\tilde{u}_s(r) = u_s(r) - \langle u_s(r) \rangle$. Considering the linearity of Eq. (21), we can assume a solution for the variable C_1 as

$$C_1 = \mathrm{Pe}\frac{\partial C_0}{\partial x}\{B_s(r) + \mathrm{Im}[B_\omega(r) e^{it_0}]\}. \tag{22}$$

Substituting Eq. (22) into Eq. (21) yields

$$\mathrm{Im}(i B_\omega e^{it_0}) + [\tilde{u}_s(r) + \mathrm{Im}(u_\omega e^{it_0})] = \frac{1}{r}\frac{d}{dr}\left(r\frac{dB_s}{dr}\right) + \mathrm{Im}\left[\frac{1}{r}\frac{d}{dr}\left(r\frac{dB_\omega}{dr}\right)e^{it_0}\right]. \tag{23}$$

In Eqs. (22) and (23), $B_s = \bar{B}_s D/a^2 u_{\mathrm{HS}}$ and $u_\omega = \bar{u}_\omega / u_{\mathrm{HS}}$. Further, B_s and B_ω depend on the solutions of two canonical problems developed using the homogenization technique, which are derived from a solution proposed to obtain a constitutive relation for the dispersion coefficient. The cell problems for the steady component B_s and for the oscillatory component B_ω are clearly obtained from Eq. (23). The steady component B_s is determined by solving the problem

$$\frac{1}{r}\frac{d}{dr}\left(r\frac{dB_s}{dr}\right) = \tilde{u}_s(r), \tag{24}$$

with the boundary conditions

$$\frac{dB_s}{dr} = 0 \quad \text{at } r = 0, 1. \tag{25}$$

For the oscillatory component B_ω, we have

$$\frac{1}{r}\frac{d}{dr}\left(r\frac{dB_\omega}{dr}\right) - iB_\omega = u_\omega(r), \tag{26}$$

with the boundary conditions

$$\frac{dB_\omega}{dr} = 0 \quad \text{at } r = 0, 1. \tag{27}$$

After defining these two cell problems, we continue developing Eq. (16), which corresponds to the $O(\epsilon^2)$ problem, to obtain the dimensionless dispersivity coefficient $\mathcal{D}$ for the PEOF with slippage at the microcapillary wall. Substituting the definition of $\tilde{u}_s$, provided above, in conjunction with Eq. (22) into Eq. (16) leads to

$$\mathrm{Pe}^2\frac{\partial^2 C_0}{\partial x^2}[\tilde{u}_s+\langle u_s\rangle+\mathrm{Im}(u_\omega e^{it_0})][B_s+\mathrm{Im}(B_\omega e^{it_0})]+\frac{\partial C_2}{\partial t_0}+\frac{\partial C_1}{\partial t_1}+\frac{\partial C_0}{\partial t_2}$$
$$=\frac{\partial^2 C_0}{\partial x^2}+\frac{1}{r}\frac{\partial}{\partial r}\left(r\frac{\partial C_2}{\partial r}\right). \tag{28}$$

Taking Eqs. (13), (20), and (22) into account, a useful expression for $\partial C_1/\partial t_1$ is as follows:

$$\frac{\partial C_1}{\partial t_1}=-\mathrm{Pe}^2\langle u_s\rangle\frac{\partial^2 C_0}{\partial x^2}[B_s+\mathrm{Im}(B_\omega e^{it_0})]. \tag{29}$$

Introducing Eq. (29) into Eq. (28) leads to

$$\mathrm{Pe}^2\frac{\partial^2 C_0}{\partial x^2}[\tilde{u}_s+\mathrm{Im}(u_\omega e^{it_0})][B_s+\mathrm{Im}(B_\omega e^{it_0})]+\frac{\partial C_2}{\partial t_0}+\frac{\partial C_0}{\partial t_2}=\frac{\partial^2 C_0}{\partial x^2}+\frac{1}{r}\frac{\partial}{\partial r}\left(r\frac{\partial C_2}{\partial r}\right). \tag{30}$$

We now take the time average over a period regarding the shortest timescale t_0 of Eq. (30). Special attention must be placed on the product $[\tilde{u}_s+\mathrm{Im}(u_\omega e^{it_0})][B_s+\mathrm{Im}(B_\omega e^{it_0})]$ at the moment to obtain its short-time average, as it can be demonstrated that the period average of the product of the two harmonic functions $\eta=\mathrm{Im}(u_\omega e^{it_0})$ and $\tau=\mathrm{Im}(B_\omega e^{it_0})$ is given by $\eta\tau=\frac{1}{2}\mathrm{Re}(u_\omega B_\omega^*)$, where $\mathrm{Re}[F]$ represents the real part of the complex quantity F and $B_\omega^*=\bar{B}_\omega^* D/a^2 u_{\mathrm{HS}}$ is the complex conjugate of B_ω. Thus, a differential equation for $\hat{C}_2$ is obtained in the form

$$\mathrm{Pe}^2\frac{\partial^2 C_0}{\partial x^2}\left[\tilde{u}_s B_s+\frac{1}{2}\mathrm{Re}(u_\omega B_\omega^*)\right]+\frac{\partial C_0}{\partial t_2}=\frac{\partial^2 C_0}{\partial x^2}+\frac{1}{r}\frac{\partial}{\partial r}\left(r\frac{\partial \hat{C}_2}{\partial r}\right), \tag{31}$$

with the boundary conditions

$$\frac{\partial \hat{C}_2}{\partial r}=0\quad\text{at } r=0,1. \tag{32}$$

Thus, a nonhomogeneous and steady boundary-value problem for $\hat{C}_2$ has been developed. Subsequently, we obtain the cross-sectionally averaged form of Eq. (31), which is defined as

$$\frac{\partial C_0}{\partial t_2}=[1+\mathrm{Pe}^2(\mathcal{D}_s+\mathcal{D}_\omega)]\frac{\partial^2 C_0}{\partial x^2}. \tag{33}$$

Here the quantity $\mathcal{E}=1+\mathrm{Pe}^2(\mathcal{D}_s+\mathcal{D}_\omega)$ represents the effective diffusivity and $\mathcal{D}\equiv\bar{\mathcal{D}}/D=\mathcal{D}_s+\mathcal{D}_\omega$ is the dimensionless effective dispersion coefficient, which is composed of two parts: a steady dispersion coefficient that depends on the deviation from the mean velocity $\mathcal{D}_s=-\langle\tilde{u}_s B_s\rangle$ and an oscillatory coefficient that depends on the periodic component of the velocity field $\mathcal{D}_\omega=-\frac{1}{2}\mathrm{Re}\langle u_\omega B_\omega^*\rangle$. Therefore, the effective dispersive coefficient can be written as

$$\mathcal{D}=-\{\langle\tilde{U}_s B_s\rangle+\tfrac{1}{2}\mathrm{Re}\langle U_\omega B_\omega^*\rangle\}. \tag{34}$$

Equation (34) represents the dispersivity of the solute on the long timescale. In the following section, we use Eq. (34) to determine the dispersion coefficient of a neutral solute in a PEOF with slippage on the inner surface of the microchannel.

III. SOLUTION METHODOLOGY

Using the methodology presented in Sec. II A, we derive the effective dispersion coefficient for a PEOF with slippage at the microcapillary wall in the following.

A. Dispersion coefficient due to the steady part of the PEOF

To obtain the steady part of $\mathcal{D}$, we first evaluate the cross-sectionally averaged velocity of the stationary component of the velocity field $u_s(r)$. From Eq. (4), the area average is

$$\langle u_s(r)\rangle = 2\int_0^1 r u_s dr = 1 - \frac{2I_1(\kappa)}{\kappa I_0(\kappa)} + \kappa\delta\frac{I_1(\kappa)}{I_0(\kappa)}. \tag{35}$$

From this result, the dimensionless velocity deviation $\tilde{u}_s$ is obtained as

$$\tilde{u}_s = u_s(r) - \langle u_s(r)\rangle = \frac{(2/\kappa)I_1(\kappa) - I_0(\kappa r)}{I_0(\kappa)}. \tag{36}$$

Considering the cell problem for B_s, Eq. (24), and Eq. (35), we obtain

$$B_s = \frac{1}{\kappa^2 I_0(\kappa)}\left[1 - I_0(\kappa r) + \frac{1}{2}\kappa r^2 I_1(\kappa)\right] + B_0. \tag{37}$$

Using the boundary conditions defined by Eq. (25), it is possible to find that B_0 is undetermined unless a unique condition is specified, which is given by

$$\langle B_s\rangle = \int_0^1 2r B_s dr = 0. \tag{38}$$

Then B_0 is obtained as

$$B_0 = \frac{(8-\kappa^2)I_1(\kappa) - 4\kappa}{4\kappa^3 I_0(\kappa)}. \tag{39}$$

Accordingly, B_s is given by

$$B_s = \frac{1}{\kappa^2 I_0(\kappa)}\left[1 - I_0(\kappa r) + \frac{1}{2}\kappa r^2 I_1(\kappa) + \frac{(8-\kappa^2)I_1(\kappa) - 4\kappa}{4\kappa}\right]. \tag{40}$$

It is now possible to define the steady component of the dispersivity $\mathcal{D}_s = \bar{\mathcal{D}}_s/D$ as follows:

$$\mathcal{D}_s = -\langle\tilde{u}_s B_s\rangle = -\frac{1}{\kappa^2 I_0^2(\kappa)}\left[I_0^2(\kappa) - \left(\frac{3}{2} + \frac{8}{\kappa^2}\right)I_1^2(\kappa) + \frac{2}{\kappa}I_0(\kappa)I_1(\kappa)\right]. \tag{41}$$

The result given by Eq. (41) was previously obtained by Ng and Zhou [11] for the dispersion coefficient of a neutral nonreacting solute due to EOF driven by a dc through a circular channel under the combined effects of longitudinal nonuniformity of potential and hydrodynamic slippage on the channel wall.

B. Dispersion coefficient due to the oscillatory part of the PEOF

We proceed to determine the oscillatory component of the dispersion coefficient. Considering the oscillatory part of the velocity profile u_ω, given by Eq. (5), and substituting it into the definition of the cell problem for B_ω, given by Eq. (26), we obtain

$$\frac{1}{r}\frac{d}{dr}\left(r\frac{dB_\omega}{dr}\right) - iB_\omega = \xi[\Gamma_2 I_0(\sqrt{iR_\omega}r) - I_0(\kappa r)]\Gamma_1. \tag{42}$$

The parameters Γ_1 and Γ_2 are defined as

$$\Gamma_1 = \frac{\kappa^2(\kappa^2 + iR_\omega)}{(\kappa^4 + R_\omega^2)I_0(\kappa)} \tag{43}$$

and

$$\Gamma_2 = \frac{I_0(\kappa) + \delta\kappa I_1(\kappa)}{I_0(\sqrt{iR_\omega}) + \delta\sqrt{iR_\omega} I_1(\sqrt{iR_\omega})}. \tag{44}$$

The solution of the cell problem (42), together with the boundary conditions given in Eq. (27), is as follows:

$$\begin{aligned} B_\omega = \frac{\xi\Gamma_1}{2(\kappa^2 - i)(iR_\omega - i)J_1(i^{3/2})}\{&\sqrt{2}\kappa(1+i)(iR_\omega - i)I_1(\kappa)J_0(i^{3/2}r) \\ &- \sqrt{2}(1+i)\Gamma_2(\kappa^2 - i)\sqrt{iR_\omega} I_1(\sqrt{iR_\omega})J_0(i^{3/2}r) \\ &- 2iJ_1(i^{3/2})[(-1+R_\omega)I_0(\kappa r) + \Gamma_2(1+i\kappa^2)I_0(\sqrt{iR_\omega}r)]\}. \end{aligned} \tag{45}$$

As described in Eq. (34), the oscillatory component of the dispersivity requires the complex conjugate of B_ω, which is represented by B_ω^* and has the form

$$\begin{aligned} B_\omega^* = \frac{\xi\Gamma_1^*}{2(\kappa^2 + i)(-iR_\omega + i)J_1\left(\frac{-1-i}{\sqrt{2}}\right)}\Bigg\{&\sqrt{2}\kappa(1-i)(-iR_\omega + i)I_1(\kappa)J_0\left(\frac{-1-i}{\sqrt{2}}r\right) \\ &- \sqrt{2}\Gamma_2^*(1-i)(\kappa^2+i)\left(\frac{1-i}{\sqrt{2}}\sqrt{R_\omega}\right)I_1\left(\frac{1-i}{\sqrt{2}}\sqrt{R_\omega}\right)J_0\left(\frac{-1-i}{\sqrt{2}}r\right) \\ &+ 2iJ_1\left(\frac{-1-i}{\sqrt{2}}\right)\left[(-1+R_\omega)I_0(\kappa r) + \Gamma_2^*(1-i\kappa^2)I_0\left(\frac{1-i}{\sqrt{2}}\sqrt{R_\omega}r\right)\right]\Bigg\}, \end{aligned} \tag{46}$$

where J_0 and J_1 are Bessel functions of order 0 and 1 of the first kind, respectively [36]. Further, Γ_1^* and Γ_2^* are the complex conjugates of Γ_1 and Γ_2, respectively, and are given by

$$\Gamma_1^* = \frac{\kappa^2(\kappa^2 - iR_\omega)}{(\kappa^4 + R_\omega^2)I_0(\kappa)} \tag{47}$$

and

$$\Gamma_2^* = \frac{I_0(\kappa) + \delta\kappa I_1(\kappa)}{I_0\left(\frac{1-i}{\sqrt{2}}\sqrt{R_\omega}\right) + \frac{1-i}{\sqrt{2}}\delta\sqrt{R_\omega} I_1\left(\frac{1-i}{\sqrt{2}}\sqrt{R_\omega}\right)}. \tag{48}$$

Therefore, the oscillatory component of the PEOF dispersivity $\mathcal{D}_\omega = -\mathrm{Re}\langle u_\omega B_\omega^*\rangle/2$ is given by the expression

$$\begin{aligned} \mathcal{D}_\omega = -\frac{1}{2}\xi^2\mathrm{Re}\Bigg(\frac{\Gamma_1\Gamma_1^*}{(\kappa^2+i)(-iR_\omega + i)J_1\left(\frac{-1-i}{\sqrt{2}}\right)}\Bigg\{&\left[\Pi_1 - \Pi_2 + 2i(\Pi_3 + \Pi_4)J_1\left(\frac{-1-i}{\sqrt{2}}\right)\right] \\ &- \left[\Pi_5 - \Pi_6 + 2i(\Pi_7 + \Pi_8)J_1\left(\frac{-1-i}{\sqrt{2}}\right)\right]\Bigg\}\Bigg). \end{aligned} \tag{49}$$

The parameters Π_j $(j = 1, \ldots, 8)$ in Eq. (49) are provided in the Appendix.

Dispersion coefficient due to the oscillatory part of the PEOF for $R_\omega = 1$

Equation (49) allows the dispersion coefficient due to the oscillatory component of the PEOF with slippage at the wall to be evaluated. In the particular case of $R_\omega = 1$, this equation is singular; however, applying l'Hôpital's rule yields

$$\lim_{R_\omega \to 1} \mathcal{D}_\omega = -\frac{1}{2}\xi^2\mathrm{Re}\left\{\sum_{j=1}^{7}\Psi_j\right\}, \tag{50}$$

with the parameters Ψ_j $(j = 1, \ldots, 7)$ provided in the Appendix.

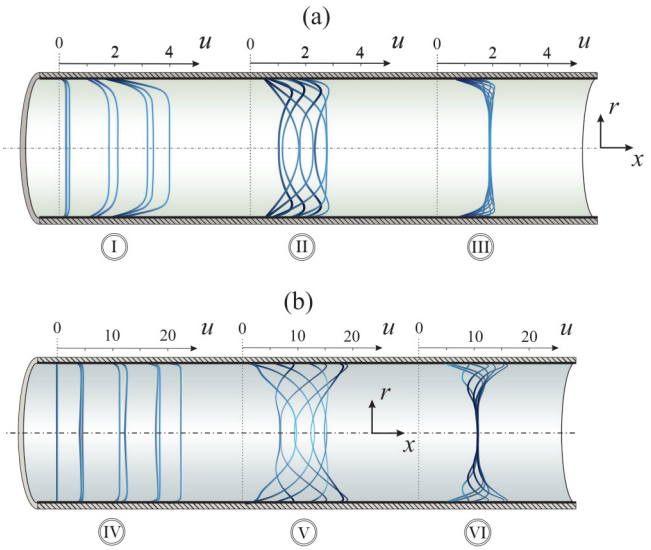

FIG. 2. Dimensionless velocity profiles caused by the PEOF in the periodic stage for $0 \leqslant t \leqslant 2\pi$ [Eq. (3)] for R_ω (=0.1, 10, and 100) with $\xi = 1.0$, $\delta = 0.1$, and two EDL thicknesses quantified by (a) $\kappa = 10$ and (b) $\kappa = 100$. Schemes I and IV correspond to $R_\omega = 0.1$, II and V to $R_\omega = 10.0$, and III and VI to $R_\omega = 100$.

IV. RESULTS AND DISCUSSION

At this point, our analytical results for the dispersion coefficient have been derived as a function of the four main parameters that control the dynamic behavior of the PEOF: κ, R_ω, ξ, and δ. To estimate the dimensionless parameters used for the calculations, a suitable combination of values for the physical parameters used in the experimental conditions reported by Green *et al.* [16], Tretheway and Meinhart [41], Dutta and Beskok [14], and Hunter [42] was selected. We begin by defining the values under consideration for the electrokinetic parameter κ, which is a dimensionless quantity that allows us to compare two characteristic length scales, i.e., the capillary radius a with respect to the Debye length λ_D, taking into account electrolyte buffer concentrations from approximately $10^{-4}M$ to $10^{-6}M$ [14,43], which correspond to Debye lengths in the range $30 \leqslant \lambda_D \leqslant 320$ nm, and also considering a radius range for the microcapillary of $10 \leqslant a \leqslant 100$ μm. Then we propose the range $10 \leqslant \kappa \leqslant 100$. The reason for the choice of the lower limit $\kappa = 10$ is to demonstrate the trends of the physical phenomena related to the PEOF's dispersion mechanism, while simultaneously considering that the Debye length must be much smaller in magnitude compared with a to avoid overlapping of the EDL developed at the boundary wall (i.e., $\kappa \gg 1$). Then we propose $\kappa = 100$ as the upper limit to exemplify this case. For the values of the angular Reynolds number, we consider that the angular frequencies ω must be kept below 1 MHz, as reported by Green *et al.* [16] in their experimental study related to EOFs driven by oscillatory electric fields. From their work, we also consider an angular frequency range $O(10^2) < \omega < O(10^4)$ Hz, and taking into account water as the solute's carrier ($\nu \sim 10^{-6}$ m^2 s^{-1}) with $10 \leqslant a \leqslant 100$ μm, we propose a dimensionless frequency range $O(10^{-1}) \lesssim R_\omega \lesssim O(10^2)$, selecting $R_\omega = 0.1$, 1, 10, and 100 as representative values. To estimate the dimensionless parameter associated with the slip length, we consider the experimental slip length reported by Tretheway and Meinhart [41], $\lambda_N = 1$ μm. Thus, to obtain the largest dimensionless slip length, we have fixed the slippage effect as $\delta = 0.1$ by considering the lower limit of the radius range. For a better understanding and support of our arguments, we present Figs. 2 and 3, along with the relevant hydrodynamical PEOF features worth considering in our discussion of the results.

We now discuss the behavior of the dispersivity coefficient $\mathcal{D}$ in terms of the dimensionless parameters involved in the analysis. Figure 4 depicts the dispersivity coefficient $\mathcal{D}$ versus the

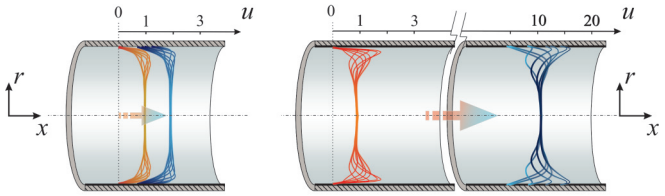

FIG. 3. Dimensionless velocity profiles caused by the PEOF in the periodic stage for $0 \leqslant t \leqslant 2\pi$ [Eq. (3)]. Red lines represent the case of no slippage with $\delta = 0$ and blue lines denote the case of slippage with $\delta = 0.1$. Both cases are plotted for $R_\omega = 100$ and (a) $\kappa = 10$ and (b) $\kappa = 100$.

electrokinetic parameter κ for values of R_ω (=0.1, 1, 10, 100) with a no-slip condition at the boundary wall ($\delta = 0$) and a fixed electric field amplitude ($\xi = 1.0$). We begin analyzing the dimensionless low-frequency curves with $R_\omega \leqslant 1$. At these low frequencies, as the flow develops in one cycle ($0 \leqslant t \leqslant 2\pi$), the resulting changes in the velocity are in phase with respect to variations in the electric field, leading to a well-defined parabolic PEOF velocity field for $k = 10$, which evolves toward the almost constant distribution typical of the pluglike profile obtained for $\kappa \to 100$ (see Fig. 2, profiles I and IV).

As shown in Fig. 4(a), for increasing values of the parameter κ, $\mathcal{D}$ is a monotonically decreasing function. This result occurs because as κ increases (or, equivalently, as the EDL thickness decreases), velocity gradients are confined to a region that is located very near the capillary wall, while a uniform distribution in the velocity dominates across the radial coordinate. This behavior leads to lower velocity gradients with a subsequent reduction in the dispersion. In the same figure, for $R_\omega = 10$ and 100, it is shown that as the EDL thickness decreases, the dispersion also decreases; however, this reduction has been attenuated in contrast with the cases of low frequencies. The factor responsible for this situation is the lagging behavior present at high frequencies between the applied electric field and the resulting velocity field. In detail, this result occurs because a unidirectional flow evolves toward a steady state through the diffusion of momentum with a characteristic timescale a^2/ν; subsequently, we can argue that when the rate of variations of the applied external electric field $E_x(t)$ (represented

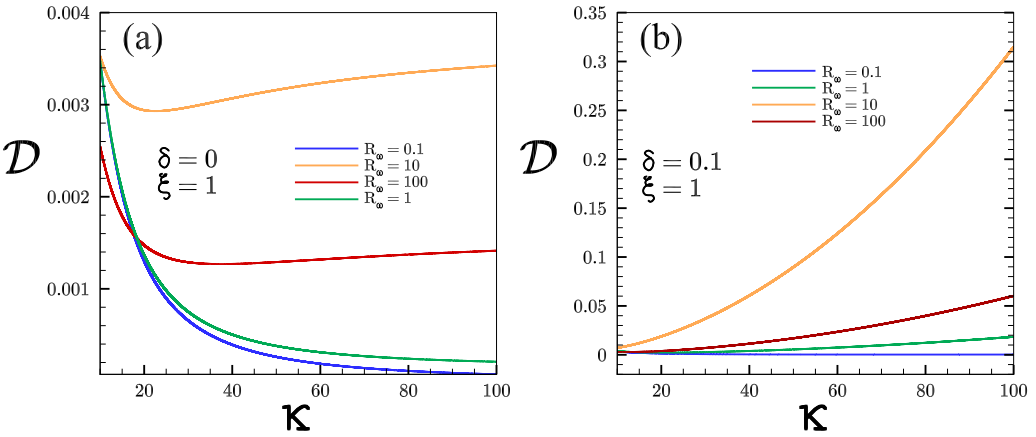

FIG. 4. Effective dispersion coefficient $\mathcal{D} = (\mathcal{E} - 1)/\mathrm{Pe}^2$ versus the electrokinetic parameter κ evaluated for four different values of the dimensionless frequency R_ω (=0.1, 1, 10, and 100). The relative amplitude of the oscillatory electric field is fixed at $\xi = 1.0$, considering (a) the no-slip condition $\delta = 0$ and (b) the Navier slip condition for $\delta = 0.1$. The curve corresponding to $R_\omega = 1.0$ has been plotted using Eq. (50).

by the timescale ω^{-1}) is slow compared with the rate of diffusion of momentum (that is, small values of R_ω, such as $R_\omega \leqslant 1$), the velocity is in a quasisteady state for each instantaneous value of E_x. Now, for values of $R_\omega \sim O(10)$ to $R_\omega \sim O(10^2)$, the electric field changes with a greater rate compared with the diffusion of momentum variations. Thus, the result is a distortion of the resulting velocity distribution with greater velocity gradients in the cross section of the microcapillary, which are not only confined to the boundary layer (see Fig. 2, velocity profiles in schemes II and V), i.e., the lagging effect acts in opposition to the influence of the EDL thickness, notably affecting the effective dispersion rate of change, and in the case of $R_\omega = 10$, the dispersion varies slightly in terms of κ. In addition, a counterintuitive feature can be observed. One could consider that as R_ω increases, then $\mathcal{D}$ will continue to improve; however, it can be observed that for $R_\omega = 100$, the dispersion curve is below that of $R_\omega = 10$. This behavior is describing a detrimental effect caused by the angular frequency of the oscillatory electric field, which can restrict the conditions for a proper solute dispersion.

Moreover, the presence of crossover frequencies (frequencies of the imposed oscillation at which the total mass transport of each species is the same [43]) can be observed, which leads us to infer the presence of the so-called crossover frequencies, a phenomenon that has previously been studied concerning the mass transport phenomena related to pressure-driven oscillatory flows with the no-slip condition at the macroscale [43] and in the field of EOF [19]. This behavior highlights the crucial role performed by oscillatory forces, which cause the fluid motion in the species separation process due to the presence of axial concentration gradients, as has been proven in the well-known analysis by Kurzweg and Jaeger [44]. Hence, we expect to find this same important role in our PEOF dispersion context. As shown in Fig. 4(a), for values in the proximity of $\kappa = 10$, the spread of a solute for low frequencies ($R_\omega \leqslant 1$) is larger than that developed for a higher frequency ($R_\omega = 100$). This feature is thoroughly explained in our $\mathcal{D}$ vs R_ω analysis.

In Fig. 4(b), we show the effect of a hydrophobic surface at the solid boundary wall on the effective dispersion coefficient. The slippage is quantified by the dimensionless parameter $\delta = 0.1$. The most pronounced feature in this case is the change in the relationship of $\mathcal{D}$ vs κ compared to the case depicted in Fig. 4(a). In contrast to the case of no slippage, the effective dispersion coefficient here is a monotonically increasing function of κ. Note that for $R_\omega \leqslant 1$, there is a slight improvement in the dispersion coefficient from $\kappa = 10$ to $\kappa = 100$. However, for increasing values of R_ω, the dispersion coefficient markedly increases between these two values, and when considering a dimensionless frequency $R_\omega = 10$, it results in an effective dispersion increase of one order of magnitude. For $R_\omega = 100$, the dispersion enhancement between these two values of κ is less remarkable; this trend describes a detriment in the rate of change of $\mathcal{D}$ caused by the dimensionless frequency, which is always present regardless of the nature of the microcapillary surface. In general, the effect of the Navier slip condition does not differ from the usual no-slip condition in a macroscale context. However, according to the results shown in Fig. 4(b), the effect on a PEOF cannot be neglected at high frequencies [$R_\omega \sim O(10), O(10^2)$]. Thus, we can argue that the presence of the slip velocity at the microcapillary wall, in conjunction with a dimensionless frequency $R_\omega \sim O(10)$ and a small EDL thickness ($k \gg 1$), favors the presence of velocity gradients through the fluid flow, which markedly affect and enhance the effective axial dispersion in the PEOF.

Equation (34) has shown that the effective dispersion coefficient is composed of two parts: a steady component $\mathcal{D}_s$, which is a function of the parameter κ, and an oscillatory part $\mathcal{D}_\omega$, which is dependent on R_ω, δ, ξ, and κ. For instance, quantifying the steady part of the effective dispersion for $\kappa = 10$ results in $\mathcal{D}_s \sim 0.002$. Meanwhile, for $\kappa = 100$, $\mathcal{D}_s \sim 5 \times 10^{-5}$ is obtained. By definition, $\mathcal{D}_s$ and $\mathcal{D}_\omega$ are positive; hence, it is possible to assert that $\mathcal{D}_s \to 0$ as $\kappa \to 100$ regardless of the nature of the microcapillary wall (the slip or no-slip condition). Subsequently, it is also possible to infer that the resulting changes in the effective dispersion $\mathcal{D}$ shown in all of our plots are practically equivalent to the corresponding variations in the oscillatory dispersion component. At this point, the strong dependence between the velocity field $u(r, t)$ and the resulting dispersion is evident; therefore, it can

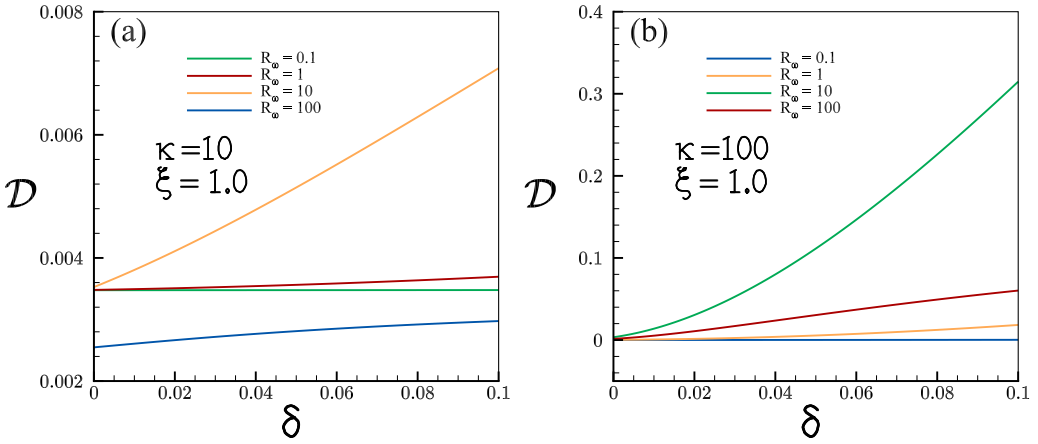

FIG. 5. Effective PEOF dispersion coefficient $\mathcal{D} = (\mathcal{E} - 1)/\mathrm{Pe}^2$ as a function of the slip length, which varies from $\delta = 0$ (no-slip condition) to $\delta = 0.1$, calculated for different values of R_ω (=0.1, 1, 10, and 100) with a relative amplitude of the oscillatory electric field of 1.0 and (a) $\kappa = 10$ and (b) $\kappa = 100$. The curve corresponding to $R_\omega = 1.0$ has been plotted using Eq. (50).

be asserted that the oscillatory component of the velocity dominates the dispersion phenomenon in the PEOF for any slip or no-slip condition considered at the boundary wall.

Next we show the effects of the slip length δ on the PEOF dispersion $\mathcal{D}$ considering different flow conditions under two EDL thicknesses, which are quantified by $\kappa = 10$ and $\kappa = 100$, as plotted in Figs. 5(a) and 5(b), respectively. Thus, varying δ on the abscissa axis is equivalent to representing the transition from a hydrophilic capillary wall toward a hydrophobic wall in a PEOF. Figure 5(a) shows that for low frequencies ($R_\omega \leqslant 1$), the nature of the microcapillary wall does not exert any influence on the effective dispersion coefficient; hence, the value of $\mathcal{D}$ varies slightly for any value of δ. For $R_\omega \sim O(10)$, a different behavior occurs; the $R_\omega = 10$ curve shows that as the slip length increases, the dispersion coefficient follows a quasilinear behavior and increases one order of magnitude compared with the case of very small values of R_ω. It can also be observed that this curve is always above the low-frequency curves, in contrast to the $R_\omega = 100$ curve, where the detrimental behavior mentioned above and a slight dispersion improvement from $\delta = 0$ to $\delta = 0.1$ are evident. Now we focus on Fig. 5(b), where we again find that under low frequencies ($R_\omega \leqslant 1$), the value of $\mathcal{D}$ becomes independent of δ; however, at the dimensionless frequency $R_\omega = 10$, a strong nonlinear dispersion enhancement between $\delta = 0$ and $\delta = 0.1$ can be observed, which is attenuated as R_ω increases. For $R_\omega = 100$, we observe an almost constant rate of change for $\mathcal{D}$ with a subsequently less remarkable dispersion enhancement.

A comparison of Figs. 5(a) and 5(b) indicates that the transition from the no-slip condition toward a finite degree of slip provides higher rates of spread when considering thick EDL thicknesses, i.e., $\kappa = 100$, for dimensionless frequencies $R_\omega > 1$. This is particularly true at $R_\omega = 10$, where it can be observed (see Fig. 7) that an increase of two orders of magnitude in the effective dispersion coefficient exists when estimated for $\delta = 0$ or $\delta = 0.1$. To justify the apparent suitability of $\kappa = 100$ with $R_\omega > 1$ for the dispersion enhancement, it is important to consider that having a slip condition at the boundary surface is defined as a reduction in the efficiency with which the wall is able to inhibit the motion of the fluid [2]. This situation is graphically depicted in Fig. 3, where the velocity profiles of the PEOF analyzed by Rojas *et al.* [32] are plotted under the assumption of zero and nonzero slip ($\delta = 0.1$) at the microcapillary wall ($\delta = 0.1$) for a dimensionless frequency $R_\omega = 100$. Note how the presence of the subsequent slip velocity promotes an increase in the mean velocity of the fluid, and for $\kappa \gg 1$, this increase is notably accentuated. Due to the strong dependence between the PEOF hydrodynamics and the effective dispersion, we find that such a pronounced flow enhancement leads to a notable

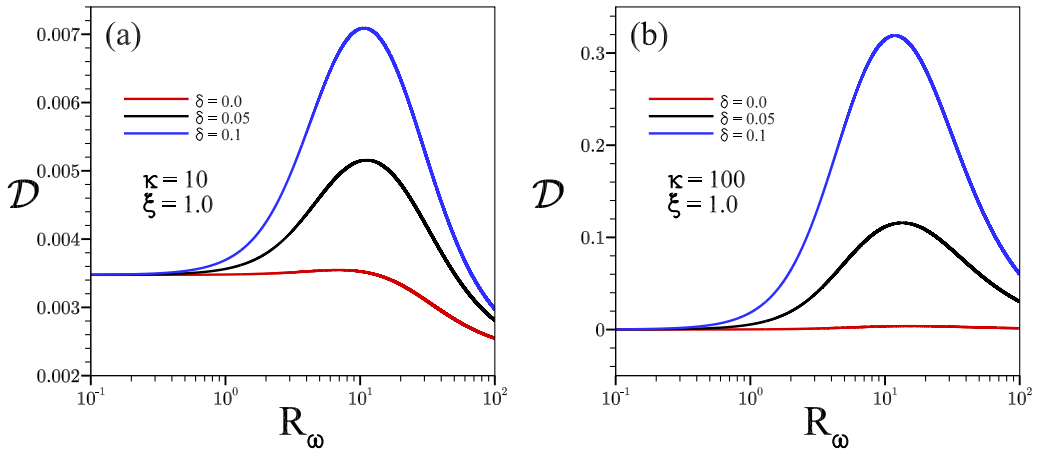

FIG. 6. Effective PEOF dispersion coefficient $\mathcal{D} = (\mathcal{E} - 1)/\mathrm{Pe}^2$ as a function of R_ω, considering also three different slip lengths at the microcapillary wall δ (=0, 0.05, and 0.1) with $\xi = 1$ and (a) $\kappa = 10$ and (b) $\kappa = 100$. For each curve, the effective dispersion coefficient corresponding to $R_\omega = 1.0$ has been calculated using Eq. (50).

increase in the effective dispersion coefficient as $\kappa \to 100$. Thus, it is possible to corroborate our assertion made based on the analysis presented in Fig. 4(b), which indicates that the hydrodynamic slippage with $\kappa \gg 1$ is an important parameter to enhance the effective dispersion coefficient, in conjunction with a dimensionless frequency $R_\omega \sim O(10)$. Another feature worth analyzing in Fig. 5 is the fact that κ appears to have an influence on the relative position of the $R_\omega = 100$ curve. For $\kappa = 10$, the $R_\omega = 100$ curve appears below the low-frequency curves ($R_\omega = 0.1$, 1). Meanwhile, for $\kappa = 100$, the $R_\omega = 100$ curve appears above the low-frequency curves. Thus, it is possible to infer that the EDL thickness can attenuate as well as reinforce the dispersion detriment trend found at frequencies of $R_\omega \sim O(10^2)$.

From our analysis developed from Figs. 4(b) and 5, we can assert that the dimensionless slip length represents a key factor in the value of the effective dispersion coefficient in a PEOF. On the one hand, for slip lengths that are different from zero, it drastically modifies the relationship between the dispersion coefficient and the EDL thickness. On the other hand, as $\kappa \to 100$ with $R_\omega > 1$, we observe a significant dispersion enhancement. However, the magnitude of this improvement appears to be conditioned by R_ω itself. Thus, the dimensionless frequency plays an important role in establishing how important this enhancement will be; however, it can contribute to deteriorating the dispersion process to such a degree that the effective dispersion for $R_\omega \sim O(10^2)$ results in being worse than that in a PEOF quasisteady state characteristic of $R_\omega \sim O(10^{-1})$ or $R_\omega \sim O(1)$. Thus, to obtain a better understanding of the effects of the dimensionless frequency on the effective dispersion, we have plotted $\mathcal{D}$ as a function of R_ω.

The curves of $\mathcal{D}$ as a function of R_ω (Figs. 6–8) are distinguished by a bell-shaped distribution. In general, such curves are composed of a constant region for low frequencies $R_\omega \leqslant 1$, where the dispersion coefficient remains practically constant. As the dimensionless frequency increases, there is a nonlinear increase in the effective dispersion coefficient until it reaches a maximum value between $R_\omega = 10$ and $R_\omega = 20$. Subsequently, the dispersion nonlinearly decreases before reaching our imposed limit at $R_\omega = 100$. This bell-shaped distribution explicitly shows the physical conditions under which the externally applied frequency ω enhances the rate of spread on the one hand and when it acts as a restrictive factor on the other.

The physical explanation for the distribution $\mathcal{D} - R_\omega$ shown in Figs. 6–8 lies in the lagging between the imposed signal of the oscillatory electric field and the resulting hydrodynamic field. In general, these curves show that as R_ω increases, the delayed fluid response respects the electrical excitement that initially exerts a positive influence on the effective dispersion, particularly at

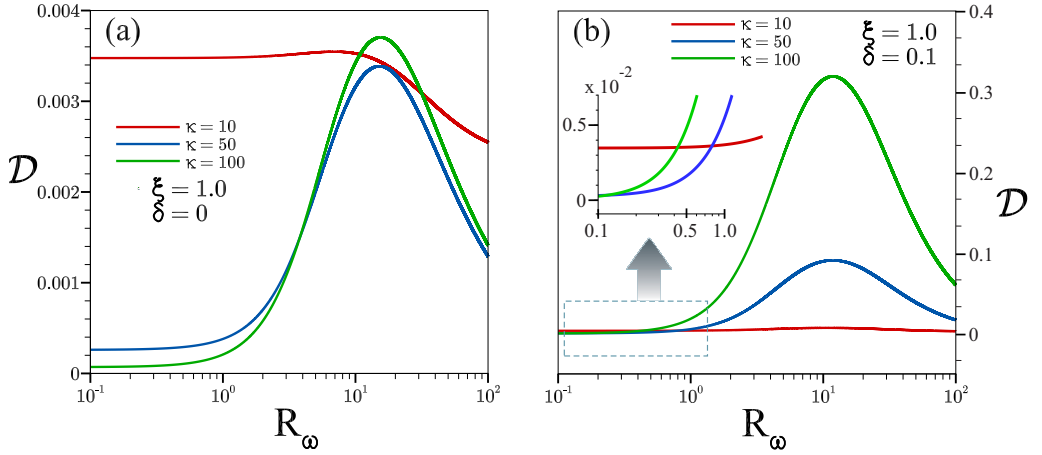

FIG. 7. Effective PEOF dispersion coefficient $\mathcal{D} = (\mathcal{E} - 1)/\mathrm{Pe}^2$ as a function of R_ω with (a) the no-slip condition and (b) the Navier slip condition, both with κ (=10, 50, and 100) and a relative amplitude of the oscillatory electric field $\xi = 1$. For each curve, the effective dispersion coefficient corresponding to $R_\omega = 1.0$ has been calculated using Eq. (50).

$R_\omega \sim O(10)$ (see Fig. 2, profiles II and V), promoting the development of important velocity gradients whose physical background was explained in Fig. 4. However, the subsequent detrimental behavior depicted for $R_\omega \sim O(10^2)$ remains to be explained. For this purpose, we must consider that the dimensionless frequency R_ω determines the importance of the inertial effects of the fluid relative to its momentum diffusion. The above means that as R_ω increases, the resistance of the fluid for achieving strong velocity variations in the core region of the microcapillary is strong. Therefore, at high frequencies, such as $R_\omega \sim O(10^2)$, this effect markedly constrains the resulting field $u(r, t)$ because it limits the instantaneous oscillations of the velocity profiles in a uniform profile, whose shape tends to be independent of the time t, mainly in the central region of the microcapillary (see Fig. 2, profiles III and VI). Consequently, the development of velocity gradients is null in

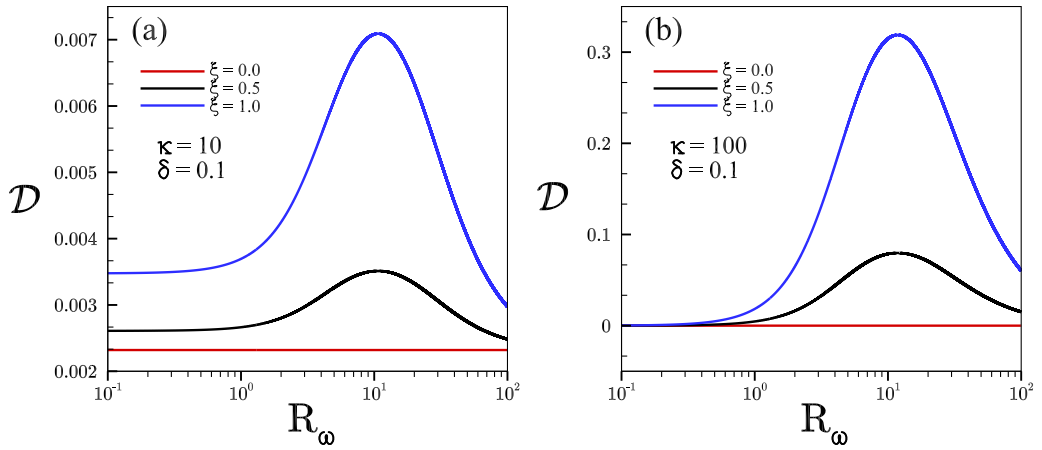

FIG. 8. Effective PEOF dispersion coefficient $\mathcal{D} = (\mathcal{E} - 1)/\mathrm{Pe}^2$ as a function of R_ω. The variation in the electric field amplitude is analyzed considering $\xi = 0$, 0.5, and 1, with the slip length at the microcapillary wall fixed at $\delta = 0.1$ for (a) $\kappa = 10$ and (b) $\kappa = 100$. For each curve, the effective dispersion coefficient corresponding to $R_\omega = 1.0$ has been calculated using Eq. (50).

the mentioned region of the capillary. The above implies that the lagging effect initially enhances the rate of spread because it contributes to reaching an optimal region for the dispersion, which is characterized by the balance between the velocity oscillations and the constraining effects proper for such a phase shift between the alternating electric field and the motion response of the fluid. This results in the highest values of $\mathcal{D}$, and finally, the lagging is so strong that it completely constrains the velocity oscillations and diminishes the resulting velocity gradients. Hence, the dispersion coefficient becomes smaller. The amplitude of this bell-shaped distribution and the corresponding magnitude of $\mathcal{D}$ depend on the nature of the slippage at the surface of the microcapillary δ, the amplitude of the imposed electric field ξ, and the electrokinetic parameter κ. The last parameter exerts some interesting effects on the relationship $\mathcal{D} - R_\omega$ that are worth discussing.

In our analysis developed for Fig. 5, we observed the influence of the parameter κ on the position of the curve $R_\omega = 100$ in the plot $\mathcal{D}$ vs δ, showing that an EDL thickness quantified by $\kappa = 10$ for $R_\omega \sim O(10^2)$ could provide effective dispersion values below those developed at lower frequencies, where there is a phase synchronization between the oscillatory electric field and the fluid response. Meanwhile, for $\kappa = 100$ and $R_\omega \sim O(10^2)$, a detrimental effect also exists, which is not drastic. The diminishing dispersion can apparently be attenuated or reinforced by the electrokinetic parameter κ. To explain this situation, we must again focus our attention on the hydrodynamic behavior of the PEOF. It has previously been shown that for $R_\omega \sim O(10^2)$, there is a uniformity in the velocity profile in the central region of the microcapillary; if we also observe Fig. 2, where the characteristic profiles for these frequencies are shown, it will be observed that the EDL thickness also has an influence on such velocity behavior and that its value determines how far from the microcapillary axis such uniformity spreads. For $\kappa = 100$ and $R_\omega = 100$ (Fig. 2, profile VI), uniform velocity profiles are constrained to the central region of the microcapillary and the region near the boundary wall is characterized by important velocity oscillations. In contrast, for $\kappa = 10$ (Fig. 2, profile III), we observe a uniform velocity in the central region of the microcapillary with less remarkable velocity gradients. Now, comparing profile III against profile I [characteristic of $R_\omega \sim O(10^{-1})$], it is clear that the first profile is more uniform than the latter; thus, more important concentration gradients caused by hydrodynamic field I than field III can be expected. Meanwhile, let us compare the flow field for $\kappa = 100$; profile VI offers larger concentration gradients than distribution IV [$R_\omega \sim O(1)$] because the uniformity in profile VI only affects the central region in the proximities of the microcapillary axis. This hydrodynamic justification is clarified through Fig. 6, where the effective dispersion coefficient shown for $R_\omega \sim O(10^2)$ can be situated below [see Fig. 6(a)] and above the dispersion values developed at $R_\omega \sim O(10^{-1})$ [see Fig. 6(b)].

Figures 6(a) and 6(b) also show the influence of the slip length variations on the curve $\mathcal{D}$ vs R_ω under two EDL conditions for $\kappa = 10$ and $\kappa = 100$, respectively. In both figures, the dispersion enhancement under the influence of the hydrodynamic slippage is evident; when a zero slip length is considered, the influence of the EDL thickness is a dominant parameter on the dispersion and, accordingly, the effective dispersion has a more relative importance for $\kappa = 10$ than for $\kappa = 100$, where the corresponding effective dispersion practically does not exist compared with the nonzero slip curves. Moreover, Fig. 6 allows us to provide more details about the influence of slippage on the dispersion in terms of the parameter R_ω to complement the slippage analysis outlined in Fig. 5. It can be observed in Figs. 6(a) and 6(b) that the presence of the slip condition at the boundary wall always represents a positive contribution to $\mathcal{D}$. However, for dimensionless frequencies $R_\omega \leqslant 1$, this contribution practically makes no difference with respect to the resulting axial dispersion developed under the no-slip condition. When considering $R_\omega > 1$, the difference between the slip condition and the no-slip condition is more evident, and for $R_\omega \sim O(10)$, we observe the highest effective dispersion coefficient regardless of the EDL thickness and the slip length values. Specifically, there is always a maximum in the interval $10 < R_\omega < 20$; additionally, note that such maxima, in conjunction with the slope of the distribution $\mathcal{D} - R_\omega$, are influenced by the dimensionless slip length value. Moreover, note that an EDL thickness quantified by $\kappa \gg 1$ with slippage at the boundary wall does not necessarily always offer a better enhancement of $\mathcal{D}$ than that of a thicker EDL (such as $\kappa = 10$). However, at dimensionless frequencies $R_\omega \sim O(10)$ and $R_\omega \sim O(10^2)$, there is a difference between

one and two orders of magnitude in the effective dispersion coefficient for $\kappa = 10$ [Fig. 6(a)] and $\kappa = 100$ [Fig. 6(b)]. Figure 7 shows that in the limit of the thin EDL thickness ($\kappa \gg 1$) and $R_\omega \sim O(10^{-1})$, the approximate solution for the hydrodynamics corresponds to a pluglike velocity profile $u = (1 + \xi \sin \hat{t})(1 + \lambda_N/\lambda_D)$, such as the one depicted in Fig. 2, scheme IV. This behavior in the velocity results in a dispersivity $\mathcal{D} \sim O(1/\kappa^2) \approx 0$ without any contribution to the molecular diffusivity, as shown in Fig. 7(b) when the green curve ($\kappa = 100$) passes by $R_\omega = 1 \times 10^{-1}$. It should be noted that the approximate solution for the velocity u in the limit of $\kappa \gg 1$ and $R_\omega \ll 1$ is the Helmholtz-Smoluchowski velocity u^s_{HS} for the quasisteady electro-osmotic flow solution under the slippage condition [32]. However, under these limits, the concave and convex fluid velocity profiles can appear inside the capillary, as Vargas *et al.* [45] have demonstrated when the magnetohydrodynamic effects are considered. Moreover, the variations in the ζ potentials of the walls would notably modify the axial distribution of the effective dispersion coefficient $\mathcal{D}$ and contribute to the molecular diffusivity, as recently reported by Arcos *et al.* [46].

The effective dispersion coefficient, as a function of R_ω, is plotted considering the no-slip condition [Fig. 7(a)] and a slip condition [Fig. 7(b)] for three values of the parameter κ. By comparing these figures, it is evident that by using a hydrophobic surface, the effective dispersion coefficient can be enhanced by two orders of magnitude in contrast to that caused by the case of the no-slip condition. Of course, this value is found when the dimensionless frequency has a value of $R_\omega \sim 10$. Another characteristic that can be observed is that in the case of $\delta = 0$ and $\kappa = 10$ [Fig. 7(a)], for almost any frequency in the range $0.1 \leqslant R_\omega \leqslant 10$, the effective dispersion coefficient remains almost constant. Additionally, Fig. 7(a) shows that as $\kappa \to 100$ and with $R_\omega < 1$, a thinner EDL layer results in a marked reduction in the already small $\mathcal{D}$ values, approximately one order of magnitude with respect to the $\kappa = 10$ curve. However, as the dimensionless frequency is increased, the characteristic bell-shaped behavior, with the enhancement or detrimental effects of the PEOF lagging, can also be observed. This behavior is more pronounced as $\kappa \to 100$; consequently, the interval $10 < R_\omega < 30$ is the range of frequencies that provide the highest dispersion values, and in this range is where a thinner EDL layer could improve the effective dispersion coefficient. Note that two crossovers occur between curves of $\kappa = 10$ and $\kappa = 100$, in the region where the peak of the bell-shaped distribution is found. Moreover, it can be observed that $\kappa = 100$ has transitioned from being the EDL condition with the worst dispersion values to offering the highest value of $\mathcal{D}$. Another crossover occurs between the curves $\kappa = 50$ and $\kappa = 100$ in Fig. 7(a) for a dimensionless frequency $3 \lesssim R_\omega \lesssim 6$.

As shown in Fig. 7(b) ($\delta = 0.1$), the notable increase in the effective dispersion coefficient is evident in comparison with the case of $\delta = 0$. The results show that the bell-shaped distribution has been scaled up to such a level that a value of $\kappa = 10$ now offers less favorable conditions for the dispersion of a solute in the PEOF. As mentioned previously, there is at least one order of magnitude between the $\mathcal{D}$ values for $\kappa = 10$ and $\kappa = 100$. However, approximately for $R_\omega < 0.4$ [see details in Fig. 7(b)], $\kappa = 10$ offers a slightly better dispersion.

Finally, the influence of the relative amplitude ξ on the effective dispersion coefficient is shown in Fig. 8. From Eq. (49), it is evident that $\mathcal{D} \sim O(\xi^2)$, which is similar to the case of an oscillatory pressure-driven flow; therefore, depending on the assumed values of ξ, it can be small in the limit $\xi \ll 1$, which means that the dispersion is dominated by the steady component of the velocity. Therefore, this figure depicts a nonlinear increase in $\mathcal{D}$ as ξ takes values of 0, 0.05, and 1. In both figures, we consider the presence of a hydrophobic surface at the microcapillary wall, but we have set $\kappa = 10$ in Fig. 8(a) and $\kappa = 100$ in Fig. 8(b). Note that for $\xi = 0$, the steady component of the dispersion is the same as the effective dispersion coefficient ($\mathcal{D}_s = \mathcal{D}$), represented by a straight line in both figures. Thus, the oscillatory component of the electric field $E_0 \xi\, \mathrm{Im}[e^{i\omega t}]$ is the main factor responsible for the resulting changes in the effective dispersion coefficient in a PEOF, which is consistent with the relevance of the oscillatory component of the velocity $u(r, t)$ shown in our analysis concerning Fig. 4. Additionally, it can be observed that $\mathcal{D}$ is independent of the changes in the electric field amplitude for $R_\omega < 1$ with $\kappa = 100$. However, for $\kappa = 10$, a dependence between ξ and the dispersion coefficient exists under such low frequencies. Although a difference between one and two orders of magnitude for $\mathcal{D}$ exists in Figs. 8(a) and 8(b) in both cases, it can be observed

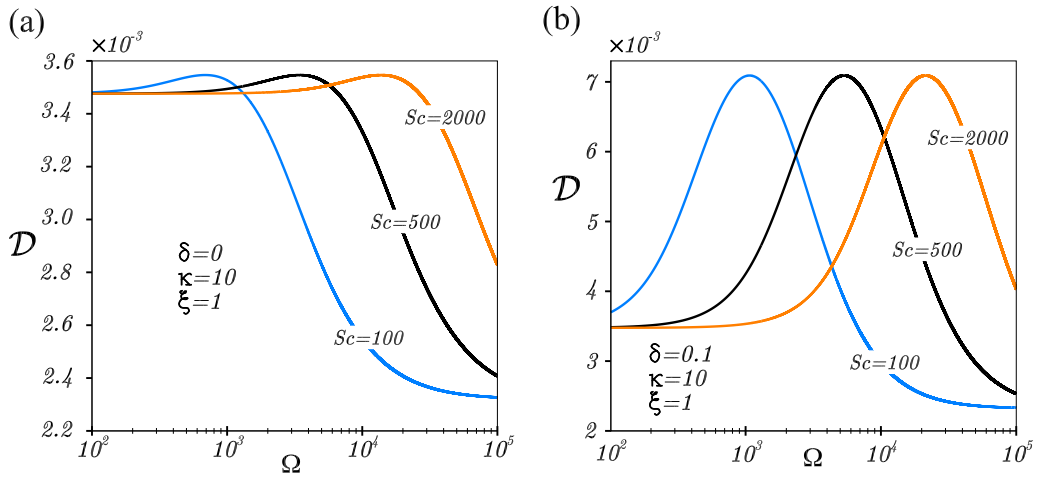

FIG. 9. Effective PEOF dispersion coefficient $\mathcal{D}$ as a function of Ω for Sc (=100, 500, and 2000) with $\kappa = 10$, $\xi = 1.0$, and (a) the no-slip condition $\delta = 0$ and (b) the slip condition $\delta = 0.1$. The points where $\mathrm{Sc} = \Omega$ were calculated considering Eq. (50) for the oscillatory dispersion component.

that the effective dispersion and its maximum are also influenced by the amplitude ξ, in addition to the parameter δ. This maximum is located in the interval $10 < R_\omega < 20$ regardless of the value of ξ.

A. Mass separation of species

To analyze the PEOF relative dispersion coefficient for the mass separation of species, as proven in the well-known analyses by Thomas and Narayanan [43] and Kurzweg and Jaeger [44], the angular Reynolds number R_ω in Eqs. (49) and (50) is replaced by $R_\omega = \Omega/\mathrm{Sc}$, where $\Omega = a^2\omega/D$ represents a dimensionless frequency referring to the transverse mass diffusion time D/a^2 and the Schmidt number $\mathrm{Sc} = \nu/D$, which relates the timescale of the diffusion of species to that of the viscous diffusion. The dispersivity of species by mass under the PEOF condition with slippage at the microcapillary wall was obtained for different values of the Schmidt number. Considering a fixed kinematic viscosity for the carrier [water, $\sim O(10^{-6})$ m^2 s^{-1}], mass diffusivities of solutes in water $D \sim O(10^{-8}$–$10^{-9})$ m^2 s^{-1}, and a typical microcapillary radius of $10 \leqslant a \leqslant 100$ μm, the Schmidt number assumes values of $\mathrm{Sc} = 100, 500, 2000$. Because $\omega < 1$ MHz [16], the frequency Ω takes values of $10^2 \leqslant \Omega \leqslant 10^5$. Curves of $\mathcal{D}$ vs Ω for $\kappa = 10$ and $\kappa = 100$ are shown in Figs. 9 and 10, respectively.

As shown in Figs. 9 and 10, as the molecular diffusion becomes smaller or the Schmidt number increases, the maximum of the bell-shaped curve moves toward the right, with a higher dimensionless frequency required to achieve the highest dispersivity. From these figures, we find that the mass dispersivity $\mathcal{D}$ of the species becomes constant as the frequency of oscillation increases from $\Omega \sim O(10^2)$ to $\Omega \sim O(10^3)$ when $\mathrm{Sc} \to 2000$, and then it proceeds to increase toward a maximum value. The mass diffusivity of the species D or the Sc does not exert any influence on the maxima of $\mathcal{D}$; however, it determines the frequency Ω at which such maxima are achieved. Regardless of the presence or absence of the slippage effect at the wall, for each Sc curve, there is a specific range of frequencies where the dispersivity is dominant over the other Sc curves. As the $\mathcal{D}$ curve tends from $\mathrm{Sc} = 2000$ to $\mathrm{Sc} = 100$, its range of dominance is located at lower frequencies Ω. For example, in Fig. 9(b), at $\Omega \approx 1 \times 10^3, 4 \times 10^3, 2 \times 10^4$, three different substances provide the same highest dispersivity values. The change in the dominance of the dispersivity of one substance over another is indicated by the crossover frequencies in Figs. 9 and 10. Figure 9(b) shows that when the slippage is present, the dispersivity $\mathcal{D}$ is approximately two times greater than when the slippage is absent [Fig. 9(a)]. By comparing Figs. 10(a) and 10(b) under conditions of slippage and $\kappa \to 100$, it is

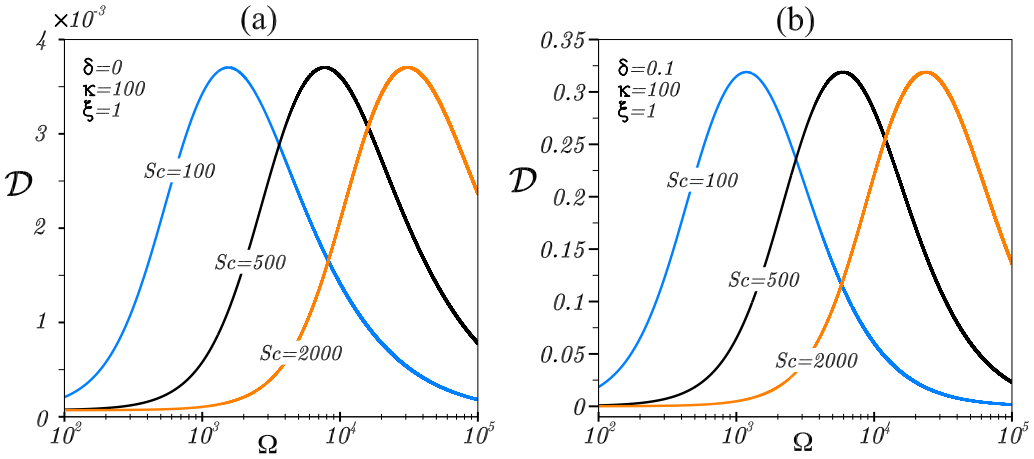

FIG. 10. Effective PEOF dispersion coefficient $\mathcal{D}$ as a function of Ω for Sc (=100, 500, and 2000) with $\kappa = 100$, $\xi = 1$, and (a) the no-slip condition $\delta = 0$ and (b) the slip condition $\delta = 0.1$. The points where $\mathrm{Sc} = \Omega$ were calculated considering Eq. (50) for the oscillatory dispersion component.

possible to confirm that the influence of the slip condition produces a difference in the dispersivity of up to two orders of magnitude with respect to the no-slippage case. We have also found that the presence of the slip condition does not exert any significant influence over the dimensionless frequency Ω at which the maximum dispersivity is achieved with respect to the no-slip condition case.

Another practical scope of our study is related to the separation ratio of two different species [47] versus Ω, for slow (like sucrose) and fast (like ethanol) diffusers in water as the carrier. The diffusivities of ethanol and sucrose in water are $D = 1.2 \times 10^{-9}$ and 0.523×10^{-9} m^2 s^{-1}, respectively. With these previous values, we found that the corresponding Schmidt numbers are $\mathrm{Sc} = 730.833$ and 1676.86, respectively. The relative dispersion coefficient as a function of the dimensionless frequency without and with the slippage condition for two different values of the electrokinetic parameter κ (=10 and 100) is shown in Figs. 11(a) and 11(b), respectively.

Figure 11(a) shows the relative dispersion coefficient $\mathcal{D}_{\mathrm{slow}}/\mathcal{D}_{\mathrm{fast}}$ for $\kappa = 10$ and for the case of $\delta = 0$ the curve shows a practically uniform behavior for lower values of Ω where the slow

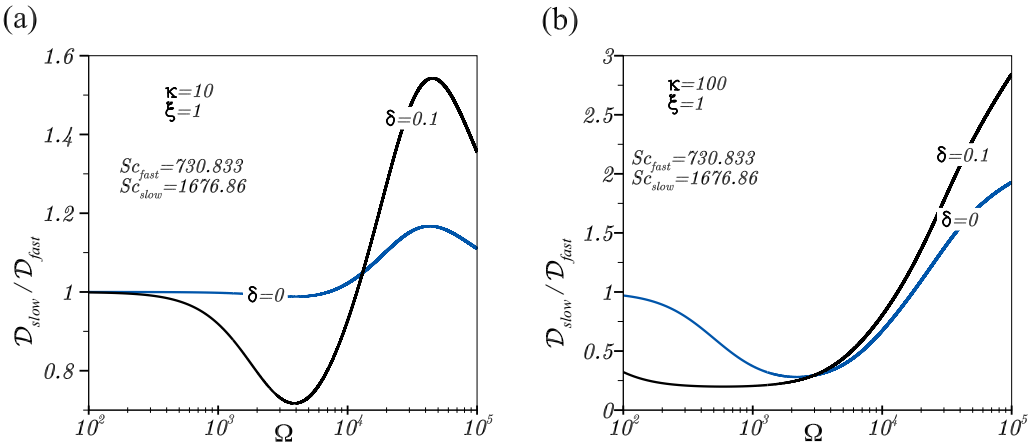

FIG. 11. Relative dispersion coefficient for a $\mathrm{Sc}_{\mathrm{slow}}$ substance (sucrose) with respect to a $\mathrm{Sc}_{\mathrm{fast}}$ substance (ethanol), under the no-slip condition $\delta = 0$ (blue curve) and with the slip condition $\delta = 0.1$ (black curve) with $\xi = 1.0$ and (a) $\kappa = 10$ and (b) $\kappa = 100$.

TABLE I. Maximum dispersivity of PEOF with and without slippage (cases 1 and 2, respectively).

Parameter	Case 1	Case 2
δ	0.1	0
R_ω	$\sim$12.0	$\sim$15.3
κ	100	100
ξ	1.0	1.0
$\mathcal{D}$	$\sim 3.2 \times 10^{-1}$	$\sim 3.7 \times 10^{-3}$

and fast diffusers have practically the same importance as the parameter Ω increases. There is a region ($\Omega \gtrsim 1 \times 10^4$) where the slow diffuser gains relevance over the fast diffuser, favoring the mass separation of species when the slippage condition is not considered (blue curve). As Ω increases, the slippage at the boundary wall represents a PEOF condition that allows the fast diffuser to gain prominence for $\Omega \leqslant O(10^4)$. There is a crossover frequency after which the slippage effect considerably enhances the importance of the slow diffuser for $\Omega \geqslant O(10^4)$ with respect to the no-slip case. This frequency is in the range $4 \times 10^4 < \Omega < 5 \times 10^4$, where we find the presence of a maximum denoting the most favorable condition for mass separation of species for the case with $\delta = 0.1$ and $\kappa = 10$. For $\kappa = 100$ [Fig. 11(b)] and $\delta = 0$ (blue curve), we have a different behavior in comparison with Fig. 11(a); in this case, as Ω increases, there is not a constant region. Instead, starting from a ratio $\mathcal{D}_{\text{slow}}/\mathcal{D}_{\text{fast}} \sim 1.0$, the slow diffuser starts to lose importance as Ω increases, and after reaching a minimum, this importance will be recovered for $\Omega \geqslant O(10^4)$. In contrast, $\kappa = 100$ with a slip condition quantified by $\delta = 0.1$ (black curve) represents two PEOF conditions that promote the importance of the slow diffuser as Ω increases from approximately $\Omega \sim O(10^3)$, favoring the mass separation of species at $\Omega \geqslant O(10^4)$. Furthermore, from Fig. 11(b), the presence of a crossover frequency after which the $\delta = 0$ and $\delta = 0.1$ curves present a similar behavior under a close range of dimensionless frequencies can be observed, after which we find a divergence favoring the dispersivity for the $\delta = 0.1$ curve. From these results, we can argue that controlling the Debye length of the EDL in addition to the electric field frequency is fundamental for the mass separation of two species with different diffusive properties diluted in a PEOF, and the slippage at the boundary wall determines how efficient this separation will be.

B. Longitudinal PEOF homogenization of solute in a microcapillary

Finally, we are interested in the longitudinal electro-osmotic homogenization of a solute in a microcapillary, where the dispersion mechanism is desirable to uniformly spread out a given portion of solute within the whole volume of a microcapillary. The transport of the solute under the influence of the molecular diffusion can be very long. For example, the time τ_m required to provide a uniform concentration of an analyte that was previously injected as a solute band is given by $\tau_m \sim L^2/D_0$, where D_0 is a reference molecular diffusion and L is the capillary length. By considering a microcapillary with a length $L = 2.5$ cm and ethanol as the analyte with $D_0 = 1.2 \times 10^{-9}$ m^2 s^{-1}, the long-scale diffusion time is $\tau_m = 5.21 \times 10^5$ s, which is equivalent to 6 d.

Now, to determine two long-scale homogenization times τ_1 considering slippage (case 1) and τ_2 without slippage (case 2) for the PEOF, we show in Table I the values of the parameters used to obtain the maximum dispersivity $\mathcal{D}$ (see also Fig. 7). Then considering an electro-osmotic velocity $u_{\text{HS}} = 0.0012$ m s^{-1}, $D = 1.2 \times 10^{-9}$ m^2 s^{-1}, and a radius of the microcapillary of 100 μm, we obtain a Pe = 100 [9]; subsequently, the effective diffusivity $\mathcal{E}$ was evaluated according to $\mathcal{E} = 1 + \text{Pe}^2\mathcal{D}$, where such effective diffusivities for cases 1 and 2 were $\mathcal{E}_1 \sim 3200$ with $\delta = 0.1$ and $\mathcal{E}_2 \sim 37$ with $\delta = 0$, respectively. Recalling that $\mathcal{E} = \bar{\mathcal{E}}/D_0$, we have $\bar{\mathcal{E}}_1 \sim 3.84 \times 10^{-6}$ m^2 s^{-1} and $\bar{\mathcal{E}}_2 \sim 4.44 \times 10^{-8}$ m^2 s^{-1}. Thus, it is possible to define two long-scale PEOF homogenization times as $\tau_1 \sim L^2/\bar{\mathcal{E}}_1 \sim 162.76$ s ($\sim$3 min) and $\tau_2 \sim L^2/\bar{\mathcal{E}}_2 \sim$

14 076.58 s (∼4 h). There are significant differences among τ_m, τ_1, and τ_2; instead of 6 d, which is required for the homogenization of a solute band due to the molecular diffusion mechanism, we have obtained a time of approximately 4 h by considering the sole influence of an external pulsatile body force inducing an EOF. However, considering a hydrophobic surface at the boundary wall of the microcapillary allows developing a time of approximately 3 min, confirming that the presence of a slip condition cannot be neglected in the PEOF microscale context.

V. CONCLUSION

In the present work, we derived an analytical expression for the effective dispersion coefficient in a PEOF with slippage at the microcapillary wall in the long-scale behavior. We can draw the following conclusions from this study.

The dimensionless frequency R_ω is a fundamental parameter that allows controlling the effective dispersion in a PEOF. For certain values of this parameter, conditions are found where there is a maximum of $\mathcal{D}$ or a detrimental behavior of it. In the present study, $R_\omega \sim O(10)$ promotes the best conditions for the effective dispersion for any fluid flow condition, regardless of the value of the dimensionless slip length δ, the relative amplitude of the oscillating electric field ξ, or the electrokinetic parameter κ.

When considering the no-slip condition at the microcapillary wall, the electrokinetic parameter κ has a marked effect on the hydrodynamics of the PEOF. This parameter exerts a dominant influence on the resulting dispersion coefficient in general and it offers the most favorable conditions for the spread of a solute when $\kappa \sim 10$. Additionally, the effects of the EDL thickness on the PEOF lagging are particularly important at high frequencies, where its influence can attenuate or accentuate the characteristic detrimental behavior of $\mathcal{D}$ associated with dimensionless frequencies $R_\omega \sim O(10^2)$.

The slip condition enhances the effective dispersion coefficient in a PEOF, particularly for $\kappa \gg 1$ and for values of $R_\omega \sim O(10)$. Considering slippage, for the same value of the relative amplitude of the oscillatory electric field, the effective dispersion coefficient can be greater by two orders of magnitude than that where the no-slip condition is assumed.

Note that in terms of the present analysis, there is a lack of support from experimental and theoretical studies and thus this issue is pending for future work. However, to validate this work, we have obtained, as a limiting case, the dispersion coefficient of an EOF driven by dc, as derived previously by Ng and Zhou [11], which is shown in Eq. (41).

ACKNOWLEDGMENTS

This work was supported by the Fondo Sectorial de Investigación para la Educación through research Grants No. CB-2013/220900 and No. CB-2011/169849 and by SIP-IPN through Grant No. 20171626. J.A. acknowledges the sabbatical research program sponsored by the Instituto Politécnico Nacional and by the CONACYT of Mexico. Additionally, J.A. acknowledges the Universidad Nacional Autónoma de México for support for making. J.M. acknowledges the CONACYT program for a master's grant at SEPI-ESIME-IPN.

APPENDIX: PARAMETERS FOR THE DISPERSION COEFFICIENT OF THE OSCILLATORY COMPONENT

The expressions (49) and (50) for D_ω involve a series of parameters, which are defined as

$$\Pi_1 = \sqrt{2}\kappa(1-i)(i-iR_\omega)I_1(\kappa)\Gamma_2 \times\left[\frac{\sqrt{iR_\omega}J_0\left(\frac{-1-i}{\sqrt{2}}\right)I_1(\sqrt{iR_\omega})+\left(\frac{-1-i}{\sqrt{2}}\right)J_1\left(\frac{-1-i}{\sqrt{2}}\right)I_0(\sqrt{iR_\omega})}{i+iR_\omega}\right], \tag{A1}$$

$$\Pi_2 = (1-i)^2(\kappa^2+i)\Gamma_2\Gamma_2^*\sqrt{R_\omega}I_1\left(\frac{1-i}{\sqrt{2}}\sqrt{R_\omega}\right) \times\left[\frac{\sqrt{iR_\omega}J_0\left(\frac{-1-i}{\sqrt{2}}\right)I_1(\sqrt{iR_\omega})+\left(\frac{-1-i}{\sqrt{2}}\right)J_1\left(\frac{-1-i}{\sqrt{2}}\right)I_0(\sqrt{iR_\omega})}{i+iR_\omega}\right], \tag{A2}$$

$$\Pi_3 = (R_\omega-1)\left[\frac{\kappa I_I(\kappa)I_0(\sqrt{iR_\omega})-\sqrt{iR_\omega}I_0(\kappa)I_1(\sqrt{iR_\omega})}{\kappa^2-iR_\omega}\right]\Gamma_2, \tag{A3}$$

$$\Pi_4 = \Gamma_2\Gamma_2^*(1-i\kappa^2)\left[\frac{\left(\frac{1-i}{\sqrt{2}}\sqrt{R_\omega}\right)I_1\left(\frac{1-i}{\sqrt{2}}\sqrt{R_\omega}\right)I_0(\sqrt{iR_\omega})-\sqrt{iR_\omega}I_0\left(\frac{1-i}{\sqrt{2}}\sqrt{R_\omega}\right)I_1(\sqrt{iR_\omega})}{-2iR_\omega}\right], \tag{A4}$$

$$\Pi_5 = \sqrt{2}\kappa(1-i)(i-iR_\omega)I_1(\kappa)\left[\frac{\kappa J_0\left(\frac{-1-i}{\sqrt{2}}\right)I_1(\kappa)+\left(\frac{-1-i}{\sqrt{2}}\right)J_1\left(\frac{-1-i}{\sqrt{2}}\right)I_0(\kappa)}{i+\kappa^2}\right], \tag{A5}$$

$$\Pi_6 = \Gamma_2^*(1-i)^2(\kappa^2+i)\sqrt{R_\omega}I_1\left(\frac{1-i}{\sqrt{2}}\sqrt{R_\omega}\right)\left[\frac{\kappa J_0\left(\frac{-1-i}{\sqrt{2}}\right)I_1(\kappa)+\left(\frac{-1-i}{\sqrt{2}}\right)J_1\left(\frac{-1-i}{\sqrt{2}}\right)I_0(\kappa)}{i+\kappa^2}\right], \tag{A6}$$

$$\Pi_7 = \frac{R_\omega-1}{2}\left[I_0^2(\kappa)-I_1^2(\kappa)\right], \tag{A7}$$

$$\Pi_8 = \Gamma_2^*(1-i\kappa^2)\left[\frac{\kappa I_0\left(\frac{1-i}{\sqrt{2}}\sqrt{R_\omega}\right)I_1(\kappa)-\left(\frac{1-i}{\sqrt{2}}\sqrt{R_\omega}\right)I_1\left(\frac{1-i}{\sqrt{2}}\sqrt{R_\omega}\right)I_0(\kappa)}{\kappa^2+iR_\omega}\right]. \tag{A8}$$

The parameters appearing in Sec. III C for the dispersion coefficient due to the oscillatory part of the PEOF, where a singularity is present in Eq. (50) at $R_\omega = 1.0$, are

$$\Psi_1 = \frac{(1-i)\kappa^5 I_1(\kappa)[I_0(\kappa)+\delta\kappa I_1(\kappa)]}{\sqrt{2}(\kappa^2+i)J_1\left(\frac{-1-i}{\sqrt{2}}\right)I_0^2(\kappa)}\left[\frac{\sqrt{i}I_1(\sqrt{i})J_0\left(\frac{1+i}{\sqrt{2}}\right)+\left(\frac{1+i}{\sqrt{2}}\right)I_0(\sqrt{i})J_1\left(\frac{1+i}{\sqrt{2}}\right)}{i(\kappa^4+1)[I_0(\sqrt{i})+\delta\sqrt{i}I_1(\sqrt{i})]}\right], \tag{A9}$$

$$\Psi_2 = -\frac{\sqrt{2}\kappa^4(1-i)(\kappa^2+i)[I_0(\kappa)+\delta\kappa I_1(\kappa)]^2}{(\kappa^2+i)J_1\left(\frac{-1-i}{\sqrt{2}}\right)I_0^2(\kappa)}\left\{\frac{\Lambda_2\Lambda_3}{\Lambda_1}+\frac{\Lambda_4}{\Lambda_1}\left(\frac{1-i}{\sqrt{2}}\right)I_1\left(\frac{1-i}{\sqrt{2}}\right)\right\}, \tag{A10}$$

$$\Psi_3 = -\frac{2\kappa^4[I_0(\kappa)+\delta\kappa I_1(\kappa)]}{(\kappa^2+i)I_0^2(\kappa)}\left\{\frac{\kappa I_0(\sqrt{i})I_1(\kappa)-(\sqrt{i})I_0(\kappa)I_1(\sqrt{i})}{(\kappa^2-i)(\kappa^4+1)[I_0(\sqrt{i})+\delta\sqrt{i}I_1(\sqrt{i})]}\right\}, \tag{A11}$$

$$\Psi_4 = \frac{\kappa^4[I_0(\kappa)+\delta\kappa I_1(\kappa)]^2}{\Lambda_5 I_0^2(\kappa)}\{\Lambda_6+\Lambda_7+\Lambda_8\}, \tag{A12}$$

$$\Psi_5 = -\frac{\sqrt{2}\kappa^5(1-i)I_1(\kappa)}{(\kappa^4+1)(\kappa^2+i)^2J_1\left(\frac{-1-i}{\sqrt{2}}\right)I_0^2(\kappa)}\left\{\kappa J_0\left(\frac{-1-i}{\sqrt{2}}\right)I_1(\kappa)+\left(\frac{-1-i}{\sqrt{2}}\right)J_1\left(\frac{-1-i}{\sqrt{2}}\right)I_0(\kappa)\right\}, \tag{A13}$$

$$\Psi_6 = \frac{\kappa^4\left[I_0^2(\kappa)-I_1^2(\kappa)\right]}{I_0^2(\kappa)(\kappa^2+i)(\kappa^4+1)}, \tag{A14}$$

$$\Psi_7 = \frac{\kappa^4[I_0(\kappa)+\delta\kappa I_1(\kappa)]}{i(\kappa^2+i)I_0^2(\kappa)J_1\left(\frac{-1-i}{\sqrt{2}}\right)}\left(\frac{\Lambda_{10}-\Lambda_{11}}{\Lambda_9}\right). \tag{A15}$$

The parameters Λ_j ($j = 1, \ldots, 11$) through (A10)–(A15) are defined through Eqs. (A16)–(A26) in the forms

$$\Lambda_1 = 2(\kappa^4+1)[I_0(\sqrt{i})+\delta\sqrt{i}I_1(\sqrt{i})]\left[I_0\left(\frac{1-i}{\sqrt{2}}\right)+\delta\left(\frac{1-i}{\sqrt{2}}\right)I_1\left(\frac{1-i}{\sqrt{2}}\right)\right], \tag{A16}$$

$$\Lambda_2 = \frac{1}{2\sqrt{2}}(1-i)I_1\left(\frac{1-i}{\sqrt{2}}\right) - \left[\frac{i}{4}I_0\left(\frac{1-i}{\sqrt{2}}\right) + I_2\left(\frac{1-i}{\sqrt{2}}\right)\right], \tag{A17}$$

$$\Lambda_3 = \sqrt{i}I_1(\sqrt{i})J_0(\sqrt{i}) + \sqrt{i}I_0(\sqrt{i})J_1(\sqrt{i}), \tag{A18}$$

$$\Lambda_4 = \frac{iI_1(\sqrt{i})J_0(\sqrt{i})}{2\sqrt{i}} + \frac{iJ_0(\sqrt{i})}{4}[I_0(\sqrt{i}) + I_2(\sqrt{i})] - \frac{1}{2\sqrt{2i}}(1-i)I_1(\sqrt{i})J_1(\sqrt{i}), \tag{A19}$$

$$\Lambda_5 = -(\kappa^4+1)[I_0(\sqrt{i}) + \delta\sqrt{i}I_1(\sqrt{i})]\left[I_0\left(\frac{1-i}{\sqrt{2}}\right) + \delta\left(\frac{1-i}{\sqrt{2}}\right)I_1\left(\frac{1-i}{\sqrt{2}}\right)\right], \tag{A20}$$

$$\Lambda_6 = -\frac{\sqrt{i}}{2}I_0\left(\frac{1-i}{\sqrt{2}}\right)I_1(\sqrt{i}) + \left[\frac{1}{2\sqrt{2}}(1-i)I_0(\sqrt{i})I_1\left(\frac{1-i}{\sqrt{2}}\right)\right], \tag{A21}$$

$$\Lambda_7 = \left[-\frac{1}{2}\sqrt{\frac{i}{2}}(1-i) + \frac{1}{2\sqrt{2i}}(1+i)\right]I_1(\sqrt{i})I_1\left(\frac{1-i}{\sqrt{2}}\right), \tag{A22}$$

$$\Lambda_8 = -\frac{i}{4}\left\{I_0\left(\frac{1-i}{\sqrt{2}}\right)[I_0(\sqrt{i}) + I_2(\sqrt{i})] + I_0(\sqrt{i})\left[I_0\left(\frac{1-i}{\sqrt{2}}\right) + I_2\left(\frac{1-i}{\sqrt{2}}\right)\right]\right\}, \tag{A23}$$

$$\Lambda_9 = -(\kappa^2+i)^2(\kappa^4+1)\left[I_0\left(\frac{1-i}{\sqrt{2}}\right) + \delta\left(\frac{1-i}{\sqrt{2}}\right)I_1\left(\frac{1-i}{\sqrt{2}}\right)\right], \tag{A24}$$

$$\Lambda_{10} = \Theta_1\left\{\frac{1}{2\sqrt{2}}(1-i)(\kappa^2+i)I_1\left(\frac{1-i}{\sqrt{2}}\right) + \left(\frac{1+i}{\sqrt{2}}\right)I_1\left(\frac{1-i}{\sqrt{2}}\right) - \frac{i}{4}(\kappa^2+i)\left[I_0\left(\frac{1-i}{\sqrt{2}}\right) + I_2\left(\frac{1-i}{\sqrt{2}}\right)\right]\right\}, \tag{A25}$$

$$\Lambda_{11} = \Theta_2\left\{-\frac{1}{2\sqrt{2}}(1-i)I_0(\kappa)I_1\left(\frac{1-i}{\sqrt{2}}\right) + \frac{\kappa}{2\sqrt{2}}(1-i)I_1(\kappa)I_1\left(\frac{1-i}{\sqrt{2}}\right) + \frac{i}{4}I_0(\kappa)\left[I_0\left(\frac{1-i}{\sqrt{2}}\right) + I_2\left(\frac{1-i}{\sqrt{2}}\right)\right]\right\}. \tag{A26}$$

In Eqs. (A25) and (A26), Θ_1 and Θ_2 have the forms

$$\Theta_1 = \sqrt{2}(1-i)(\kappa^2+i)\left[\kappa J_0\left(\frac{-1-i}{\sqrt{2}}\right)I_1(\kappa) + \left(\frac{-1-i}{\sqrt{2}}\right)J_1\left(\frac{-1-i}{\sqrt{2}}\right)I_0(\kappa)\right], \tag{A27}$$

$$\Theta_2 = 2i(\kappa^2+i)(1-i\kappa^2)J_1\left(\frac{-1-i}{\sqrt{2}}\right). \tag{A28}$$

[1] G. I. Taylor, Dispersion of soluble matter in solvent flowing slowly through a tube, Proc. R. Soc. London Ser. A **219**, 186 (1953).

[2] L. G. Leal, *Advanced Transport Phenomena* (Cambridge University Press, Cambridge, 2007).

[3] R. Aris, On the dispersion of a solute in pulsating flow through a tube, Proc. R. Soc. London Ser. A **259**, 370 (1960).

[4] P. C. Chatwin, On the longitudinal dispersion of passive contaminant in oscillatory flows in tubes, J. Fluid Mech. **71**, 513 (1975).

[5] E. J. Watson, Diffusion in oscillatory pipe flow, J. Fluid Mech. **133**, 233 (1983).

[6] J. Lee, E. Kulla, A. Chauhan, and A. Tripathi, Taylor dispersion in polymerase chain reaction in a microchannel, Phys. Fluids **20**, 093601 (2008).

[7] J. Lee, A. Tripathi, and A. Chauhan, Taylor dispersion in oscillatory flow in rectangular channels, Chem. Eng. Sci. **117**, 183 (2014).

[8] H. A. Stone, A. D. Stroock, and A. Ajdari, Engineering flows in small devices: Microfluidics toward a laboratory-on-a-chip, Annu. Rev. Fluid Mech. **36**, 381 (2004).
[9] N.-T. Nguyen, *Micromixers: Fundamentals, Design and Fabrication*, 2nd ed. (William Andrew, Norwich, 2011).
[10] A. D. Stroock, S. K. Dertinger, A. Ajdari, I. Mezić, H. A. Stone, and G. M. Whitesides, Chaotic mixer for microchannels, Science **295**, 647 (2002).
[11] C. O. Ng and Q. Zhou, Dispersion due to electroosmotic flow in a circular microchannel with slowly varying wall potential and hydrodynamic slippage, Phys. Fluids. **24**, 112002 (2012).
[12] S. Datta and S. Ghosal, Characterizing dispersion in microfluidic channels, Lab Chip **9**, 2537 (2009).
[13] S. Ghosal, Electrokinetic flow and dispersion in capillary electrophoresis, Annu. Rev. Fluid Mech. **38**, 309 (2006).
[14] P. Dutta and A. Beskok, Analytical solution of time periodic electroosmotic flows: Analogies to Stokes' second problem, Anal. Chem. **73**, 5097 (2001).
[15] S. Chakraborty and S. Ray, Mass flow-rate control through time periodic electro-osmotic flows in circular microchannels, Phys. Fluids **20**, 083602 (2008).
[16] N. G. Green, A. Ramos, A. Gonzalez, H. Morgan, and A. Castellanos, Fluid flow induced by nonuniform ac electric fields in electrolytes on microelectrodes. I. Experimental measurements, Phys. Rev. E **61**, 4011 (2000).
[17] S. Bhattacharyya and A.K. Nayak, Time periodic electro-osmotic transport in a charged micro/nano channel, Colloid. Surf. A **325**, 152 (2008).
[18] M. H. Oddy, J. G. Santiago, and J. C. Mikkelsen, Electrokinetic instability micromixing, Anal. Chem. **73**, 5822 (2001).
[19] H. F. Huang and C. L. Lai, Enhancement of mass transport and separation of species by oscillatory electroosmotic flows, Proc. R. Soc. A **462**, 2017 (2006).
[20] G. Ramon, Y. Agnon, and C. Dosoretz, Solute dispersion in oscillating electro-osmotic flow with boundary mass exchange, Microfluid. Nanofluid. **10**, 97 (2011).
[21] J. Song and C. O. Ng, Dispersion in oscillatory electro-osmotic flow through a parallel-plate channel with kinetic sorptive exchange at walls, J. Hydrodyn. B **26**, 363 (2014).
[22] S. Paul and C. O. Ng, Dispersion in electroosmotic flow generated by oscillatory electric field interacting with oscillatory wall potentials, Microfluid. Nanofluid. **12**, 237 (2012).
[23] C.-O. Ng and Q. Zhou, Electro-osmotic flow through a thin channel with gradually varying wall potential and hydrodynamic slippage, Fluid Dyn. Res. **44**, 055507 (2012).
[24] A. Matías, S. Sánchez, F. Méndez, and O. Bautista, Influence of slip wall effect on a non-isothermal electro-osmotic flow of a viscoelastic fluid, Int. J. Therm. Sci. **98**, 352 (2015).
[25] Q. Zhou and C.-O. Ng, Electro-osmotic dispersion in a circular tube with slip-stick striped wall, Fluid Dyn. Res. **47**, 015502 (2015).
[26] E. Lauga, M. Brenner, and H. Stone, *Microfluidics: The No-Slip Boundary Condition* (Springer, Berlin, 2007).
[27] S. S. Bahga, O. I. Vinogradova, and M. Z. Bazant, Anisotropic electro-osmotic flow over super-hydrophobic surfaces, J. Fluid. Mech. **644**, 245 (2010).
[28] J. Jamaati, H. Niazmand, and M. Renksizbulut, Pressure-driven electrokinetic slip-flow in planar microchannels, Int. J. Therm. Sci. **49**, 1165 (2010).
[29] L. Joly, C. Ybert, E. Trizac, and L. Bocquet, Hydrodynamics within the Electric Double Layer on Slipping Surfaces, Phys. Rev. Lett. **93**, 257805 (2004).
[30] D. M. Huang, C. Cottin-Bizonne, C. Ybert, and L. Bocquet, Massive Amplification of Surface-Induced Transport at Superhydrophobic Surfaces, Phys. Rev. Lett. **101**, 064503 (2008).
[31] H. M. Park and T. W. Kim, Extension of the Helmholtz-Smoluchowski velocity to the hydrophobic microchannels with velocity slip, Lab Chip **9**, 291 (2009).
[32] G. Rojas, J. Arcos, M. Peralta, F. Méndez, and O. Bautista, Pulsatile electroosmotic flow in a microcapillary with the slip boundary condition, Colloid Surf. A **513**, 57 (2017).
[33] J. Chakraborty, S. Ray, and S. Chakraborty, Role of streaming potential on pulsating mass flow rate control in combined electroosmotic and pressure-driven microfluidic devices, Electrophoresis **33**, 419 (2012).

[34] M. Peralta, J. Arcos, F. Méndez, and O Bautista, Oscillatory electroosmotic flow in a parallel- plate microchannel under asymmetric zeta potentials, Fluid Dyn. Res. **49**, 035514 (2017).
[35] R. F. Probstein, *Physicochemical Hydrodynamics: An Introduction* (Wiley, New York, 1994).
[36] *NIST Handbook of Mathematical Functions*, edited by F. W. J. Olver, D. W. Lozier, R. F. Boisvert, and C. W. Clark (Cambridge University Press, Cambridge, 2010).
[37] J. Happel and H. Brenner, *Low Reynolds Number Hydrodynamics: With Special Applications to Particulate Media* (Kluwer, Dordrecht, 1983).
[38] C. C. Mei and B. Vernescu, *Homogenization Methods for Multiscale Mechanics* (World Scientific, Singapore, 2010).
[39] C. C. Mei, J. L. Auriault, and C. O. Ng, Some applications of the homogenization theory, Adv. Appl. Mech. **32**, 277 (1996).
[40] C. O. Ng, Dispersion in steady and oscillatory flows through a tube with reversible and irreversible wall reactions, Proc. R. Soc. A **462**, 481 (2006).
[41] D. C. Tretheway and C. D. Meinhart, Apparent fluid slip at hydrophobic microchannel walls, Phys. Fluids **14**, L9 (2002).
[42] R. J. Hunter, *Zeta Potential in Colloid Science: Principles and Applications* (Academic, New York, 1981).
[43] A. M. Thomas and R. Narayanan, Physics of oscillatory flow and its effect on the mass transfer and separation of species, Phys. Fluids **13**, 859 (2001).
[44] U. H. Kurzweg and M. J. Jaeger, Diffusional separation of gases by sinusoidal oscillations, Phys. Fluids **30**, 1023 (1987).
[45] C. Vargas, J. Arcos, O. Bautista, and F. Méndez, Hydrodynamic dispersion in a combined magnetohydrodynamic-electroosmotic-driven flow through a microchannel with slowly varying wall zeta potentials, Phys. Fluids **29**, 092002 (2017).
[46] J. C. Arcos, F. Méndez, E. G. Bautista, and O. Bautista, Dispersion coefficient in an electro-osmotic flow of a viscoelastic fluid through a microchannel with a slowly varying wall zeta potential, J. Fluid Mech. **839**, 348 (2018).
[47] A. Hacioglu and R. Narayanan, Oscillating flow and separation of species in rectangular channels, Phys. Fluids **28**, 073602 (2016).